Synthesis, Reactivity, and Catalytic Behavior of Iron/Zinc-Containing Species Involved in Oxidation of Hydrocarbons under Gif-Type Conditions

Bharat Singh,[†] Jeffrey R. Long,[‡] Fabrizia Fabrizi de Biani,[§] Dante Gatteschi,[§] and Pericles Stavropoulos*,[†]

Contribution from the Departments of Chemistry, Boston University, Boston, Massachusetts 02215, Harvard University, Cambridge, Massachusetts 02138, and Università degli Studi di Firenze, I-50144 Florence, Italy

Abstract: The present study explores the nature and reactivity of iron- and zinc-containing species generated in hydrocarbon-oxidizing Gif[IV]-type solutions (Fe catalyst/Zn/O_2 in pyridine/acetic acid (10:1 v/v). The ultimate goal of this investigation is to unravel the role of metal sites in mediating dioxygen-dependent C−H activation, which in the case of Gif chemistry demonstrates an enhanced selectivity for the ketonization of secondary carbons. Reaction of $[Fe_3O(O_2CCH_3)_6(py)_3]$·py (**1**) with zinc powder in CH_3CN/CH_3COOH or CH_2Cl_2/CH_3COOH affords the trinuclear compound $[Zn_2Fe^{II}(O_2CCH_3)_6(py)_2]$ (**2**). Single-crystal X-ray analysis confirms that one monodentate and two bidentate acetate groups bridge adjacent pairs of metals with the iron atom occupying a centrosymmetric position. The analogous reduction of **1** in py/CH_3COOH (10:1, 5:1, 2:1 v/v) yields $[Fe^{II}(O_2CCH_3)_2(py)_4]$ (**3**), $[Fe^{II}_2(O_2CCH_3)_4(py)_3]_n$ (**4**), and $[Zn(O_2CCH_3)_2(py)_2]$ (**5**) depending on the isolation procedure employed. Compound **3** possesses a distorted octahedral geometry, featuring a C_2 axis bisecting the equatorial, pyridine-occupied plane, whereas the two acetate groups reside along the perpendicular axis. Compound **4** is a one-dimensional solid constructed by asymmetric diferrous units. Two bidentate and one monodentate acetate groups bridge the two iron sites, with the monodentate bridge also acting as a chelator to one ferrous center. The two iron centers exhibit weak antiferromagnetic coupling. Compounds **3** and **4** are also accessible from the reduction of **1** with iron powder or treatment with H_2/Pd. Solutions of **3** and **4** in pyridine or py/CH_3COOH react with pure dioxygen or air to eventually regenerate **1** in a concentration-dependent manner. Oxidation of **2** in py/CH_3COOH with pure dioxygen or air yields $[Fe_{2.22(2)}Zn_{0.78(2)}O(O_2CCH_3)_6(py)_3]$·py (**1′**) and $[Zn_2(O_2CCH_3)_4(py)_2]$ (**6**). Compound **1′** is isostructural to **1,** exhibiting rhombohedral symmetry at 223 K. The filtrate of the reduction of **1** with zinc in neat pyridine, when exposed to dioxygen, affords dichroic red−green crystals of monoclinic $[Fe_2ZnO(O_2CCH_3)_6(py)_3]$·py (**1″**). Species **1″** yields products identical with those provided by **1** under reducing conditions. Compounds **2**−**6** are related by pyridine-dependent equilibria, as demonstrated by mutual interconversions and electronic absorption data in pyridine and py/CH_3COOH solutions. In non-pyridine solutions, Zn-containing species **5** and **6** rearrange to the crystallographically characterized species $[Zn(O_2CCH_3)_2(py)]_n$ (**7**) and $[Zn_3(O_2CCH_3)_6(py)_2]$ (**8**). Compound **7** is a one-dimensional solid featuring a chain of Zn sites linked by a bidentate acetate group while additionally coordinated by a chelating acetate. Compound **8** is isostructural to **2**. Further perturbations of the described structures are apparent in ionic iron-containing species, such as the pseudo-seven-coordinate iron in $[Ph_3P=N=PPh_3][Fe^{II}(O_2CCH_3)_3(py)]$ (**9**), which is obtained from the reaction of **3** with $[PPN][O_2CCH_3]$, and the water-coordinated iron in $[Fe^{II}(H_2O)_4(trans\text{-}py)_2][O_2CCH_3]_2$ (**10**), which reveals an extensive two-dimensional network of hydrogen-bonding interactions. The pyridine-free species $[Fe^{II}_3(O_2CCH_3)_6(OS(CD_3)_2)_2]_n$ (**11**) is isolable upon extensive incubation of **3** in $(CD_3)_2SO$. Compound **11** exhibits a remarkable one-dimensional structure, featuring four different types of acetate groups. Catalytic oxidations of adamantane, iso-pentane, benzene, toluene, *cis*-stilbene, and pyridine mediated by the system **1** (or **2**−**4**)/Zn/O_2 in py/AcOH (10:1) afford product profiles which are not fully compatible with the reported outcome of analogous oxidations by hydroxyl radicals or biologically relevant high-valent iron−oxo species alone. The intermolecular deuterium kinetic isotope effect for the oxidation of adamantane to adamantanone is small ($k_H/k_D = 2.01(12)$) by comparison to values obtained for oxidation of hydrocarbons by biological oxygenases. Employment of hydrogen peroxide, *t*-BuOOH, or peracetic acid as potential oxo donors does not provide viable shunt pathways in the catalytic oxygenation of adamantane. The nature of active oxidant in Gif[IV]-type oxidation is discussed in light of these structural and functional findings.

Introduction

A substantial number of non-heme, iron-containing biological sites[1] have recently emerged as required or circumstantial centers in dioxygen transport and activation. Both mononuclear[2] and dinuclear[3] iron centers have been firmly recognized to reside in a protein cavity in which a putative ferric (alkyl/hydro)peroxo

and/or a high-valent iron−oxo intermediate is generated upon dioxygen activation. Of particular interest in this context is the currently emerging[4] dinuclear $Fe^{III/IV}−(\mu\text{-}O)_2−Fe^{IV}$ core and its precursor $Fe^{III}−(\mu\text{-}O_2)−Fe^{III}$ moiety that may prove to be as versatile active oxidants in non-heme diiron systems as the

---
[†] Boston University.
[‡] Harvard University.
[§] Università degli Studi di Firenze.
[⊗] Abstract published in *Advance ACS Abstracts,* July 1, 1997.

(1) (a) Feig, A. L.; Lippard, S. J. *Chem. Rev.* **1994**, *94*, 759−805. (b) Que, L., Jr. In *Bioinorganic Catalysis*; Reedijk, J., Ed.; Marcel Dekker: New York, 1993; pp 347−393. (c) Wilkins, R. G. *Chem. Soc. Rev.* **1992**, *21*, 171−178. (d) Vincent, J. B.; Olivier-Lilley, G. L.; Averill, B. A. *Chem. Rev.* **1990**, *90*, 1447−1467. (e) Que, L., Jr.; True, A. E. *Prog. Inorg. Chem.* **1990**, *38*, 97−200. (f) Kurtz, D. M., Jr. *Chem. Rev.* **1990**, *90*, 585−606. (g) Lippard, S. J. *Angew. Chem., Int. Ed. Engl.* **1988**, *27*, 344−361.

putative $Fe^{IV}=O$/residue$^{+\bullet}$ unit has been in heme iron chemistry.[5] In principle, potent oxidants of this kind can execute substrate oxygenation/desaturation[6] or generate a biologically beneficial[7] (and occasionally detrimental)[8] long-lived radical upon interaction with biological material. Reactive oxygen species (superoxide, singlet oxygen, alkoxyl/hydroxyl radicals, nitric oxide)[9] have also been implicated in degenerative biological oxidations[10] via mechanisms involving, *inter alia*, mediation by inadvertently present iron (or copper) ions.

One inspirational example of hydroxylating activity is the remarkable oxidation of methane to methanol mediated by the well-documented diiron site of the hydroxylase component of soluble methane monooxygenase (sMMO). The crystal structures[6a,b] (2.2 Å (4.0 °C) and 1.7 Å (−160 °C) resolution) of the "as isolated" (H_{ox}) and dithionite-reduced (H_{red}) hydroxylase protein from *Methulococcus capsulatus* (Figure 1), as well as the recent structure (2.0 Å (−18 °C)) of the H_{ox} protein from *Methylosinus trichosporium* OB3b,[3,4b] have revealed the presence of a hydroxo-bridged diiron center in H_{ox} (Fe⋯Fe = 3.4/3.1 Å at 2.2/1.7 Å resolution) and a hydroxo-devoid diiron site in H_{red} (Fe⋯Fe = 3.28 Å). The lack of hydroxyl bridge in H_{red} is coordinatively compensated by a unique carboxylate shift (Glu 243) from a terminal (H_{ox}) to a monodentate-bridging as well as chelating position. In addition, the bridging water molecule in H_{ox} (1.7 Å resolution structure; a buffer-derived bidentate acetate is occupying this position in the 2.2 Å resolution structure) assumes a nearly terminal position, with only a long-range interaction with the other iron atom in H_{red}.
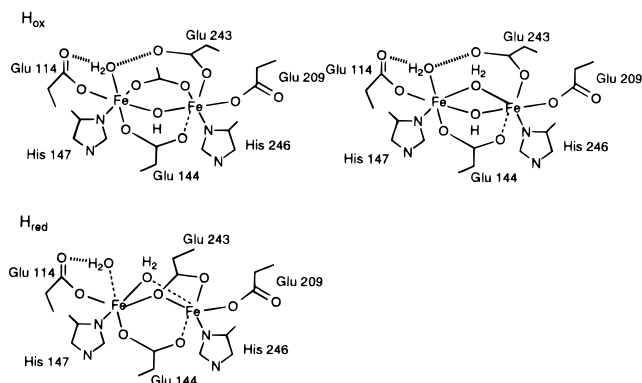

Figure 1. Structures of H_{ox} (2.2 Å (4.0 °C) and 1.7 Å (−160 °C) resolution) and H_{red} of sMMO from *M. capsulatus* (after Rosenzweig, A. C.; et al. *Chem. Biol.* **1995**, *2*, 409−418).[6a]

Concomitantly, the terminal water molecule in H_{ox} is almost dissociated in H_{red}. These atomic translocations upon reduction lead to a core structure that is nearly five-coordinate at the iron sites, although the semivacant coordination positions are at orthogonal orientations.

Synthetic analogues of dinuclear iron sites[11] have been instrumental in elucidating structural aspects pertaining to the enzymatic center of sMMO, but instances of functional behavior are scarce.[12] The latter category includes hydrocarbon-oxidizing systems such as $[Fe_2O(TPA)_2(H_2O)_2]^{4+}$/$t$-BuOOH($H_2O_2$),[13,14] $[Fe_2O(L)_4X_n]^{m+}$/t-BuOOH (L = 2,2′-bipy, 4,4′-Me$_2$-2,2′-bipy, 1,10-phen; X = H$_2$O, Cl, OAc, CF$_3$CO$_2$),[15] $[Fe_2O(OAc)_2(bipy)_2$-Cl$_2$]/t-BuOOH(H_2O_2),[16] $[Fe_2O(OAc)(tmima)_2]^{3+}$/$H_2O_2$,[16a] $[Fe_2O$-$(H_2O)_2$-(tmima)$_2]^{4+}$/H_2O_2,[17] $[Fe_2O(HB(pz)_3)_2(X)_2]$/Zn/O$_2$ (X = OAc, hfacac),[18] and $[Fe_2O(salen)_2]$/2-mercaptoethanol/O$_2$.[19] Although only a handful of these systems employ dioxygen, some of those featuring alternative oxo donors have been established to operate via a dioxygen-dependent pathway.[13a]

(2) (a) Que, L., Jr.; Ho, R. Y. N. *Chem. Rev.* **1996**, *96*, 2607−2624. (b) Kappock, T. J.; Caradonna, J. P. *Chem. Rev.* **1996**, *96*, 2659−2756.

(3) Wallar, B. J.; Lipscomb, J. D. *Chem. Rev.* **1996**, *96*, 2625−2657.

(4) (a) Que, L., Jr.; Dong, Y. *Acc. Chem. Res.* **1996**, *29*, 190−196. (b) Shu, L.; Nesheim, J. C.; Kauffmann, K.; Münck, E.; Lipscomb, J. D.; Que, L., Jr. *Science* **1997**, *275*, 515−518. (c) Liu, K. E.; Valentine, A. M.; Wang, D.; Huynh, B. H.; Edmondson, D. E.; Salifoglou, A.; Lippard, S. J. *J. Am. Chem. Soc.* **1995**, *117*, 10174−10185.

(5) (a) Sono, M.; Roach, M. P.; Coulter, E. D.; Dawson, J. H. *Chem. Rev.* **1996**, *96*, 2841−2887. (b) *Cytochrome P-450: Structure, Mechanism, and Biochemistry*; Montellano, P. O., Ed.; Plenum Press: New York, 1986.

(6) sMMO: (a) Rosenzweig, A. C.; Nordlund, P.; Takahara, P. M.; Frederick, C. A.; Lippard, S. J. *Chem. Biol.* **1995**, *2*, 409−418. (b) Rosenzweig, A. C.; Frederick, C. A.; Lippard, S. J.; Nordlund, P. *Nature* **1993**, *366*, 537−543. Toluene 2- and 4-Monooxygenases: (c) Newman, L. M.; Wackett, L. P. *Biochemistry* **1995**, *34*, 14066−14076. (d) Pikus, J. D.; Studts, J. M.; Achim, C.; Kauffmann, K. E.; Münck, E.; Steffan, R. J.; McClay, K.; Fox, B. G. *Biochemistry* **1996**, *35*, 9106−9119. Stearoyl-acyl carrier protein Δ⁹ desaturase: (e) Fox, B. G.; Shanklin, J.; Somerville, C.; Münck, E. *Proc. Natl. Acad. Sci. U.S.A.* **1993**, *90*, 2486−2490. Rybrerythrin: (f) deMaré, F.; Kurtz, D. M., Jr.; Nordlund, P. *Nature Struct. Biol.* **1996**, *3*, 539−546. (g) Gupta, N.; Bonomi, F.; Kurtz, D. M., Jr.; Ravi, N.; Wang, D. L.; Huynh, B. H. *Biochemistry* **1995**, *34*, 3310−3318. Phenol hydroxylase: (h) Nordlund, I.; Powlowski, J.; Shingler, V. *J. Bacteriol.* **1990**, *172*, 6826−6833. Xylene monooxygenase and alkane hydroxylase: (i) Shanklin, J.; Whittle, E.; Fox, B. G. *Biochemistry* **1994**, *33*, 12787−12794. Ferroxidase center of ferritin: (j) Harrison, P. M.; Arosio, P. *Biochim. Biophys. Acta* **1996**, *1275*, 161−203.

(7) Ribonucleotide reductase: (a) Logan, D. T.; Su, X.-D.; Åberg, A.; Regnström, K.; Hadju, J.; Eklund, H.; Nordlund, P. *Structure* **1996**, *4*, 1053−1064. (b) Nordlund, P.; Eklund, H. *J. Mol. Biol.* **1993**, *232*, 123−164. (c) Nordlund, P.; Sjöberg, B.-M.; Eklund, H. *Nature* **1990**, *345*, 593−598. (d) Ravi N.; Bollinger, J. M., Jr.; Huynh, B. H.; Edmondson, D. E.; Stubbe, J. *J. Am. Chem. Soc.* **1994**, *116*, 8007−8014. (e) Bollinger, J. M., Jr.; Tong, W. H.; Ravi, N.; Huynh, B. H.; Edmondson, D. E.; Stubbe, J. *J. Am. Chem. Soc.* **1994**, *116*, 8015−8023.

(8) (a) Pogozelski, W. K.; McNeese, T. J.; Tullius, T. D. *J. Am. Chem. Soc.* **1995**, *117*, 6428−6433. (b) Cheng, C.-C.; Goll, J. G.; Neyhart, G. A.; Welch, T. W.; Singh, P.; Thorp, H. H. *J. Am. Chem. Soc.* **1995**, *117*, 2970−2980. (c) Stadtman, E. R. *Science* **1992**, *257*, 1220−1224. (d) Minotti, G.; Aust, S. D. *Lipids* **1992**, *27*, 219−226.

(9) (a) Sawyer, D. T. *Oxygen Chemistry*; Oxford University Press: New York, 1991; pp 120−187. (b) Stamler, J. S.; Singel, D. J.; Loscalzo, J. *Science* **1992**, *258*, 1898−1902.

(10) (a) Halliwell, B.; Gutteridge, J. M. C. *Free Radicals in Biology and Medicine*; Clarendon Press: Oxford, U.K., 1989; pp 22−85. (b) von Sonntag, C. *The Chemical Basis of Radiation Biology*; Taylor & Francis: London, 1987; pp 394−428. (c) Garrison, W. M. *Chem. Rev.* **1987**, *87*, 381−398.

(11) Herold, S.; Lippard, S. J. *J. Am. Chem. Soc.* **1997**, *119*, 145−156 and references therein.

(12) (a) Stassinopoulos, A.; Mukerjee, S.; Caradonna, J. P. In *Mechanistic Bioinorganig Chemistry*; Thorp, H. H., Pecoraro, V. L., Eds.; American Chemical Society: Washington, DC, 1995; pp 83−120. (b) Caradonna, J. P.; Stassinopoulos, A. *Adv. Inorg. Biochem.* **1994**, *9*, 245−315.

(13) (a) Kim, J.; Harrison, R. G.; Kim, C.; Que, L., Jr. *J. Am. Chem. Soc.* **1996**, *118*, 4373−4379. (b) Kim, J.; Larka, E.; Wilkinson, E. C.; Que, L., Jr. *Angew. Chem., Int. Ed. Engl.* **1995**, *34*, 2048−2051. (c) Kojima, T.; Leising, R. A.; Yan, S.; Que, L., Jr. *J. Am. Chem. Soc.* **1993**, *115*, 11328−11335. (d) Leising, R. A.; Kim, J.; Perez, M. A.; Que, L., Jr. *J. Am. Chem. Soc.* **1993**, *115*, 9524−9530.

(14) Abbreviations used: TPA, tris(2-pyridylmethyl)amine; tmima, tris-((1-methylimidazol-2-yl)methyl)amine; HB(pz)$_3$, hydrotris(pyrazolyl)borate; hfacac, hexafluoroacetylacetone; salen, N,N′-bis(salicylidene)ethylenediamine; EDTA, ethylenediamine-N,N,N′,N′-tetraacetate; ATR, attenuated total internal reflectance; PPN, bis(triphenylphosphine)iminium; Me$_3$-TACN, 1,4,7-trimethyl-1,4,7-triazacyclononane; ICP, inductively coupled plasma; ⁱPrOx, bis[2-((4S)-(1-methylethyl)-1,3-oxazolinyl)]methane; PheMe$_3$Eda, N,N,N′-trimethyl-N′-[4,4-dimethyl-4-(3,5-di-*tert*-butyl-4-hydroxyphenyl)butyl]ethylenediamine; BIPhMe, bis(1-methyl-2-imidazolyl)phenylmethoxymethane; BIPhOH, bis(1-methyl-2-imidazolyl)phenylhydroxymethane; BIDPhEH, 1,1-bis(1-methyl-2-imidazolyl)-1-(3,5-di-*tert*-butyl-4-hydroxyphenyl)ethane; CumOOH, cumene hydroperoxide; PAH, picolinic acid.

(15) (a) Ménage, S.; Wilkinson, E. C.; Que, L., Jr.; Fontecave, M. *Angew. Chem., Int. Ed. Engl.* **1995**, *34*, 203−205. (b) Ménage, S.; Vincent, J. M.; Lambeaux, C.; Chottard, G.; Grand, A.; Fontecave, M. *Inorg. Chem.* **1993**, *32*, 4766−4773.

(16) (a) Fish, R. H.; Konings, M. S.; Oberhausen, K. J.; Fong, R. H.; Yu, W. M.; Christou, G.; Vincent, J. B.; Coggin, D. K.; Buchanan, R. M. *Inorg. Chem.* **1991**, *30*, 3002−3006. (b) Vincent, J. B.; Huffman, J. C.; Christou, G.; Li, Q.; Nanny, M. A.; Hendrickson, D. N.; Fong, R. H.; Fish, R. H. *J. Am. Chem. Soc.* **1988**, *110*, 6898−6900.

(17) Buchanan, R. M.; Chen, S.; Richardson, J. F.; Bressan, M.; Forti, L.; Morvillo, A.; Fish, R. H. *Inorg. Chem.* **1994**, *33*, 3208−3209.

(18) (a) Kitajima, N.; Ito, M.; Fukui, H.; Moro-oka, Y. *J. Chem. Soc., Chem. Commun.* **1991**, 102−104. (b) Kitajima, N.; Fukui, H.; Moro-oka, Y. *J. Chem. Soc., Chem. Commun.* **1988**, 485−486.

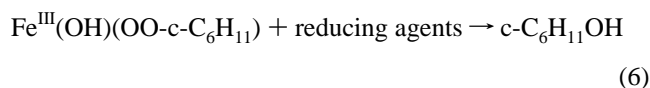(19) Tabushi, I.; Nakajima, T.; Seto, K. *Tetrahedron Lett.* **1980**, *2*, 2565−2568.
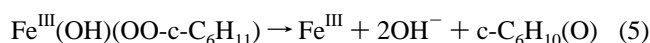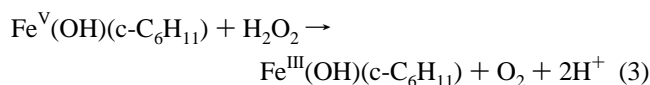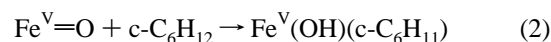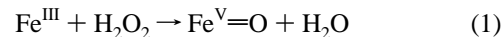
However, the nature of the active oxidant(s) involved has remained largely unspecified or is a matter of debate.

On the other hand, iron species that have received less attention as structurally competent mimics have nonetheless been long implicated in celebrated hydrocarbon-oxidizing systems, such as the century-old Fenton reagent (Fe^{II}/H$_2$O$_2$, aqueous (pH 2))[20] and the more biologically relevant, dioxygen-dependent Udenfriend (Fe^{II}/EDTA/ascorbate/O$_2$)[21] and Gif[22] systems. Gif chemistry has achieved notoriety owing to its superior product yield and selectivity as well as its potential biomimetic value. The catalysts involved in Gif solutions[23] operate primarily in pyridine/acetic acid (py/AcOH) and consist of an Fe$^{II/III}$ salt, dioxygen or simply air, and a coreducing agent (Fe, Zn, electrochemical cathode) or the equivalent Fe^{III}/H$_2$O$_2$ and Fe^{III}/ *t*-BuOOH (60 °C) combinations. Additives such as picolinic acid (PAH) can substantially enhance the rate of the reaction.[24] Typical reagents employing PAH include combinations such as FeCl$_3$/PAH/H$_2$O$_2$ (1:4:4) in pyridine or py/AcOH (10:1) and Fe^{II}(PA)$_2$/H$_2$O$_2$ (1:20) in py/AcOH (2:1). Copper-based Gif catalysts have also been reported.[25]

The proposed mechanistic pathways purported to account for the suggested selectivity of Gif systems vis-à-vis hydrocarbon substrates (sec > tert > prim) deviate from current mechanistic considerations as applied to P-450[5,26] or sMMO[4,27] biological sites. These mechanisms further reflect the continuing debate with respect to the nature of the active oxidant involved, namely whether it is metal-based or simply a reactive oxygen species (hydroxyl/alkoxyl radical). The mode of C−H activation by the putative oxidant (concerted or radical) has remained equally controversial.

The original Barton mechanism,[22] pertaining to the homogeneous Fe^{III}/H$_2$O$_2$ system, includes the formation of an iron oxenoid species (assuming a mononuclear site), as well as a number of intriguing but rather unusual steps (eqs 1−6; illustrated for cyclohexane) such as formation of organometallic intermediates and insertion of O$_2$ into Fe−C bonds. The latter has been suggested to account for the observation that substrate oxygenation is dioxygen dependent. The major products are ketones and a small amount of secondary alcohols, both suggested to arise from a common metal−alkylperoxy moiety by spontaneous decomposition and action of reducing agents, respectively. A key finding in this context is the detection of cyclohexylhydroperoxide[23] as an intermediate in the oxidation of cyclohexane, slowly decomposing to cyclohexanone and cyclohexanol. The involvement of *sec*-alkyl radicals has been excluded on the basis of the absence of scavenger-trapped products, especially in the form of coupled *sec*-alkylpyridines.[28] Competitive experiments[29] employing the Fe^{II}/H$_2$O$_2$ and Fe^{III}/

H$_2$O$_2$ combinations in the presence of substrate and excess chloride have indicated that the former system deviates toward generation of alkyl radicals (trapped as alkyl chlorides) while the latter exclusively affords ketones, thus showing no signs of alkyl radical formation.

$$Fe^{III} + H_2O_2 \rightarrow Fe^V{=}O + H_2O \qquad (1)$$

$$Fe^V{=}O + c\text{-}C_6H_{12} \rightarrow Fe^V(OH)(c\text{-}C_6H_{11}) \qquad (2)$$

$$Fe^V(OH)(c\text{-}C_6H_{11}) + H_2O_2 \rightarrow$$
$$Fe^{III}(OH)(c\text{-}C_6H_{11}) + O_2 + 2H^+ \quad (3)$$

$$Fe^{III}(OH)(c\text{-}C_6H_{11}) + O_2 \rightarrow Fe^{III}(OH)(OO\text{-}c\text{-}C_6H_{11}) \qquad (4)$$

$$Fe^{III}(OH)(OO\text{-}c\text{-}C_6H_{11}) \rightarrow Fe^{III} + 2OH^- + c\text{-}C_6H_{10}(O) \quad (5)$$

$$Fe^{III}(OH)(OO\text{-}c\text{-}C_6H_{11}) + \text{reducing agents} \rightarrow c\text{-}C_6H_{11}OH$$
$$(6)$$

More recent interpretations[29] of the FeCl$_3$/PAH/H$_2$O$_2$ system, favor generation of a diferric Fe^{III}−(μ-O$_2$)−Fe^{III} unit that is subsequently converted to the oxenoid Fe^{III}−(μ-O$_2$)−Fe^V{=}O moiety by reaction with 1 equiv of H$_2$O$_2$. Alternative active oxidants such as [Fe(OOH)(O$_2$)(PA)$_2$(pyH$^+$)] have been proposed[30] by virtue of product-profile similarities observed between "oxygenated Fenton" (Fe^{II}(PA)$_2$/H$_2$O$_2$ (1:20) in py/AcOH (2:1)) and Gif systems, and corresponding discrepancies found between these metal-based systems and genuine hydroxyl radical oxidations.[20b] However, none of the alleged intermediates have been rigorously detected.

In contrast, the more traditional radical version of this mechanism has been proposed by Minisci[31] to account at least for Gif chemistry employing *t*-BuOOH. Alkoxyl radicals have been postulated as being the active oxidant, generated by Fe^{II}-dependent decomposition of *t*-BuOOH. The required Minisci steps (eqs 7−15) predict a ketone:alcohol ratio of ≥1. Product selectivity may be influenced by the solvent-dependent competitive rates of eqs 9−10. Corroborative evidence for the operation of the radical mechanism has been provided by Ingold and co-workers[32] for Gif-type chemistry involving a variety of alkylhydroperoxides. These and related studies[33] have been instrumental in demonstrating the ubiquitous nature of alkoxyl and alkylperoxyl radicals in metal-mediated oxidations by *t*-BuOOH.[34] Analogous interpretations[31b,35] pertaining to catalytic oxidations mediated by P-450-type mimics coupled to alkylhydroperoxides have been similarly cautious in regards to the

(20) (a) Walling, C. *Acc. Chem. Res.* **1975**, *8*, 125−131. (b) Sawyer, D. T.; Kang, C.; Llobet, A.; Redman, C. *J. Am. Chem. Soc.* **1993**, *115*, 5817−5818.

(21) Udenfriend, S.; Clark, C. T.; Axelrod, J.; Brodie, B. B. *J. Biol. Chem.* **1954**, *208*, 731−739.

(22) Barton, D. H. R.; Doller, D. *Acc. Chem. Res.* **1992**, *25*, 504−512.

(23) Barton, D. H. R.; Bévière, S. D.; Chavasiri, W.; Csuhai, E.; Doller, D.; Liu, W.-G. *J. Am. Chem. Soc.* **1992**, *114*, 2147−2156.

(24) (a) Balavoine, G.; Barton, D. H. R.; Boivin, J.; Gref, A. *Tetrahedron Lett.* **1990**, *3*, 659−662. (b) Tung, H.-C.; Kang, C.; Sawyer, D. T. *J. Am. Chem. Soc.* **1992**, *114*, 3445−3455.

(25) (a) Barton, D. H. R.; Bévière, S. D.; Chavasiri, W.; Csuhai, E.; Doller, D. *Tetrahedron* **1992**, *48*, 2895−2910. (b) Barton, D. H. R.; Csuhai, E.; Doller, D. *Tetrahedron Lett.* **1992**, *33*, 4389−4392.

(26) (a) McMurry, T. J.; Groves, J. T. In ref 5b, pp 1−28. (b) Groves, J. T. In *Metal Ion Activation of Dioxygen*; Spiro, T. G., Ed.; Wiley: New York, 1980; pp 125−162. (c) Groves, J. T. *J. Chem. Educ.* **1985**, *62*, 928−931. (d) Newcomb, M.; Le Tadic-Biadatti, M.-H.; Chestney, D. L.; Roberts, E. S.; Hollenberg, P. F. *J. Am. Chem. Soc.* **1995**, *117*, 12085−12091.

(27) (a) Liu, K. E.; Johnson, C. C.; Newcomb, M.; Lippard, S. J. *J. Am. Chem. Soc.* **1993**, *115*, 939−947. (b) Choi, S.-Y., Eaton, P. E.; Hollenberg, P. F.; Liu, K. E.; Lippard, S. J.; Newcomb, M.; Putt, D. A.; Upadhyaya, S. P.; Xiong, Y. *J. Am. Chem. Soc.* **1996**, *118*, 6547−6555.

(28) Barton, D. H. R.; Halley, F.; Ozbalik, N.; Schmitt, M.; Young, E.; Balavoine, G. *J. Am. Chem. Soc.* **1989**, *111*, 7144−7149.

(29) Barton, D. H. R.; Hu, B.; Taylor, D. K.; Rojas Wahl, R. U. *J. Chem. Soc., Perkin Trans. 2* **1996**, 1031−1041.

(30) Sawyer, D. T.; Sobkowiak, A.; Matsushita, T. *Acc. Chem. Res.* **1996**, *29*, 409−416.
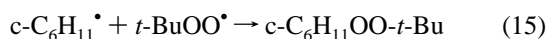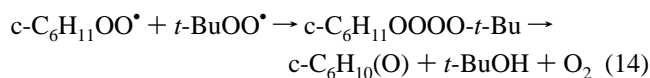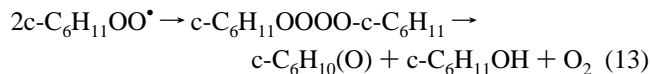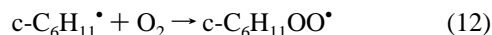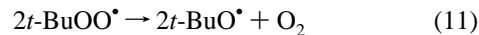
(31) (a) Minisci, F.; Fontana, F.; Araneo, S.; Recupero, F. *J. Chem. Soc., Chem. Commun.* **1994**, 1823−1824. (b) Minisci, F.; Fontana, F.; Araneo, S.; Recupero, F.; Banfi, S.; Quici, S. *J. Am. Chem. Soc.* **1995**, *117*, 226−232. (c) Minisci, F.; Fontana, F. *Tetrahedron Lett.* **1994**, *35*, 1427−1430. (d) Minisci, F.; Fontana, F.; Araneo, S.; Recupero, F.; Zhao, L. *Synlett* **1996**, 119−125.

(32) Snelgrove, D. W.; MacFaul, P. A.; Ingold, K. U.; Wayner, D. D. M. *Tetrahedron Lett.* **1996**, *37*, 823−826.

(33) (a) Arends, I. W. C. E.; Ingold, K. U.; Wayner, D. D. M. *J. Am. Chem. Soc.* **1995**, *117*, 4710−4711. (b) MacFaul, P. A.; Arends, I. W. C. E.; Ingold, K. U.; Wayner, D. D. M. *J. Chem. Soc., Perkin Trans. 2* **1997**, 135−145.

(34) (a) Nguyen, C.; Guajardo, R. J.; Mascharak, P. K. *Inorg. Chem.* **1996**, *35*, 6273−6281. (b) Rabion, A.; Chen, S.; Wang, J.; Buchanan, R. M.; Seris, J.-L.; Fish, R. H. *J. Am. Chem. Soc.* **1995**, *117*, 12356−12357.

active oxidant involved.

$$Fe^{II} + t\text{-BuOOH} \rightarrow Fe^{III} + OH^- + t\text{-BuO}^\bullet \quad (7)$$

$$Fe^{III} + t\text{-BuOOH} \rightarrow Fe^{II} + H^+ + t\text{-BuOO}^\bullet \quad (8)$$

$$t\text{-BuO}^\bullet + c\text{-C}_6H_{12} \rightarrow t\text{-BuOH} + c\text{-C}_6H_{11}^\bullet \quad (9)$$

$$t\text{-BuO}^\bullet + t\text{-BuOOH} \rightarrow t\text{-BuOH} + t\text{-BuOO}^\bullet \quad (10)$$

$$2t\text{-BuOO}^\bullet \rightarrow 2t\text{-BuO}^\bullet + O_2 \quad (11)$$

$$c\text{-C}_6H_{11}^\bullet + O_2 \rightarrow c\text{-C}_6H_{11}OO^\bullet \quad (12)$$

$$2c\text{-C}_6H_{11}OO^\bullet \rightarrow c\text{-C}_6H_{11}OOOO\text{-}c\text{-C}_6H_{11} \rightarrow$$
$$c\text{-C}_6H_{10}(O) + c\text{-C}_6H_{11}OH + O_2 \quad (13)$$

$$c\text{-C}_6H_{11}OO^\bullet + t\text{-BuOO}^\bullet \rightarrow c\text{-C}_6H_{11}OOOO\text{-}t\text{-Bu} \rightarrow$$
$$c\text{-C}_6H_{10}(O) + t\text{-BuOH} + O_2 \quad (14)$$

$$c\text{-C}_6H_{11}^\bullet + t\text{-BuOO}^\bullet \rightarrow c\text{-C}_6H_{11}OO\text{-}t\text{-Bu} \quad (15)$$
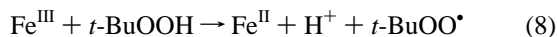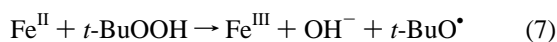
Alternative metal-based active oxidants, that have been suggested by Barton[29] to form alkyl radicals, include the couple $Fe^{II}-OOH/Fe^{IV}=O$, generated by the competitive Fe^{II}/H_2O_2 combination under dioxygen-deficient conditions. The alkyl radical is proposed to be the product of homolytic cleavage within an $HO-Fe^{IV}-R$ unit.

The relationship between Gif chemistry and sMMO activity relies on potential structural similarities due to the choice of solvents (py/AcOH) in Gif catalysis and the nature of amino acid residues of the diiron site in sMMO. However, functional analogies are much more tentative and need to be carefully examined. Despite the fact that the peculiar Gif-type selectivity parallels the one encountered in the activity of sMMO for a limited number of substrates,[36,37] the following discrepancies exist: (i) Gif catalysts mediate mostly ketonization of secondary carbons[38] while sMMO features hydroxylation of primary carbons;[39] (ii) oxidation of olefins leads largely to ketonization in Gif chemistry,[22] as opposed to mostly stereospecific epoxidation by sMMO[37b] and P-450[5a] systems; (iii) radical-clock experiments indicate[40] the presence of diffusively free (long-lived) alkyl radicals in $t\text{-BuOOH}/H_2O_2$-based Gif chemistry, but only short-lived (<100 fs) substrate radicals under P-450[26d] or

sMMO[27a] oxidations, although results obtained[27a,41] with sMMO from *M. trichosporium* suggest longer life spans for the generated alkyl radicals; and (iv) deuterium primary kinetic isotope effect (KIE) values tend to be low (≤ 2.5)[42] in Gif-type oxidations by comparison to intrinsic KIE values for hydroxylations catalyzed by P-450 isozymes/mimics (KIE = $10-14$;[5a] more modest and disperse values have also been measured[43]) and sMMO[27a] (KIE values larger than 50 have been reported[44] for methane with *M. trichosporium*, although ethane exhibits a value of 4).

To gain a more intimate view of the role of metal sites in Gif-type chemistry as well as explore possible connectivities with structural/functional aspects pertaining to sMMO, we have turned our attention to Gif^{IV}-type systems (Fe$^{II/III}$/O$_2$/Zn/substrate in py/AcOH) with emphasis on the basic iron acetate [Fe$_3$O(O$_2$-CCH$_3$)$_6$(py)$_3$]·py (**1**) as starting material and catalyst. Several lines of evidence make the choice of this mixed-valent species attractive: (i) the metal ligation (Fe$-$O = 1.9 Å, Fe$\cdots$Fe = 3.4 Å)[45] is representative of corresponding moieties and metrical parameters in H$_{ox}$ of sMMO;[6a] (ii) the ferrous site in **1** can be readily replaced[45] by a non-redox ion such as Mg^{2+} or Zn^{2+}, practically reducing the species to a dinuclear iron compound; (iii) compound **1** has been isolated[46] from catalytic mixtures and successfully used[47] as a source of iron in Gif-type oxidation of hydrocarbons (Gif^{IV}); and (iv) the all-ferric [Fe$_3$O(O$_2$CCH$_3$)$_6$-(py)$_3$]$^+$ is reported[48] to mediate epoxidation of olefins by molecular oxygen.

The following are pertinent questions that need to be progressively addressed in this study: (i) What are the characteristics of the reduced iron sites that may be accountable for dioxygen binding and activation during catalytic turnovers? (ii) What are the products of autoxidation of these reduced species upon exposure to dioxygen? (iii) Are there any discernible structural similarities that may allow us to draw legitimate analogies between iron centers present in Gif-type solutions and at the active site of sMMO? (iv) How does the product profile of substrate oxidations mediated by the **1**/Zn/ O$_2$ system, and variations thereof, compare in terms of yield, regio(chemo)specificity, and KIE values to other Fenton- and Gif-type systems as well as to sMMO and P-450 hydroxylase activity? (v) Is there any evidence that the isolable "catalysts" are kinetically competent to mediate substrate oxidation and can intermediates of dioxygen activation be detected and related to substrate turnover?

Answers to questions i$-$iv are investigated in this article. Question v needs to be addressed on the basis of the results of a comprehensive kinetic study coupled with a systematic search for the detection of intermediates. Such work is currently in

(35) (a) Mansuy, D.; Bartoli, J.-F.; Momenteau, M. *Tetrahedron Lett.* **1982**, *23*, 2781$-$2784. (b) Mansuy, D.; Bartoli, J.-F.; Chottard, J.-C.; Lange, M. *Angew. Chem., Int. Ed. Engl.* **1980**, *19*, 909$-$910. (c) Ledon, H. *C. R. Hebd. Seances Acad. Sci., Ser. C* **1979**, *288*, 29$-$31. (d) Baccouche, M.; Ernst, J.; Fuhrhop, J.-H.; Schlözer, R.; Arzoumanian, H. *J. Chem. Soc., Chem. Commun.* **1977**, 821$-$822. (e) Meunier, B. *Chem. Rev.* **1992**, *92*, 1411$-$1456.

(36) (a) Barton, D. H. R.; Boivin, J.; Motherwell, W. B.; Ozbalik, N.; Schwartzentruber, K. M.; Jankowski, K. *New J. Chem.* **1986**, *10*, 387$-$398. (b) Sheu, C.; Sobkowiak, A.; Zhang, L.; Ozbalik, N.; Barton, D. H. R.; Sawyer, D. T. *J. Am. Chem. Soc.* **1989**, *111*, 8030$-$8032. (c) Sheu, C.; Richert, S. A.; Cofré, P.; Ross, B., Jr.; Sobkowiak, A.; Zhang, L.; Sawyer, D. T.; Kanofsky, J. R. *J. Am. Chem. Soc.* **1990**, *112*, 1936$-$1942.

(37) (a) Froland, W. A.; Andersson, K. K.; Lee, S.-K.; Liu, Y.; Lipscomb, J. D. *J. Biol. Chem.* **1992**, *267*, 17588$-$17597. (b) Green, J.; Dalton, H. *J. Biol. Chem.* **1989**, *264*, 17698$-$17703.

(38) However, in the presence of reducing agents, Gif systems can operate as hydroxylation catalysts without significant competition by the presumably more easily oxidized reducing additive (this has been termed the "Gif paradox"); see ref 23.

(39) Apparently, the predilection toward hydroxylation of primary sites is not native to the hydroxylase component of sMMO but is significantly influenced by the presence of the regulatory protein B. For a discussion, see ref 37a.

(40) Newcomb, M.; Simakov, P. A.; Park, S.-U. *Tetrahedron Lett.* **1996**, *37*, 819$-$822.

(41) Ruzicka, F.; Huang, D.-S.; Donnelly, M. I.; Frey, P. A. *Biochemistry* **1990**, *29*, 1696$-$1700.

(42) Barton, D. H. R.; Doller, D.; Geletii, Y. V. *Tetrahedron Lett.* **1991**, *32*, 3811$-$3814.

(43) Sorokin, A.; Robert, A.; Meunier, B. *J. Am. Chem. Soc.* **1993**, *115*, 7293$-$7299 and references therein.

(44) (a) Nesheim, J. C.; Lipscomb, J. D. *Biochemistry* **1996**, *35*, 5, 10240$-$10247. (b) Nesheim, J. C.; Lipscomb, J. D. *J. Inorg. Biochem.* **1995**, *59*, 369.

(45) Cannon, R. D.; White, R. P. *Prog. Inorg. Chem.* **1988**, *36*, 195$-$298. (b) Woehler, S. E.; Wittebort, R. J.; Oh, S. M.; Kambara, T.; Hendrickson, D. N.; Inniss, D.; Strouse, C. E. *J. Am. Chem. Soc.* **1987**, *109*, 1063$-$1072.

(46) Barton , D. H. R.; Gastiger, M. J.; Motherwell, W. B. *J. Chem. Soc., Chem. Commun.* **1983**, 731$-$733.

(47) Barton, D. H. R.; Boivin, J.; Gastiger, M.; Morzycki, J.; Hay-Motherwell, R. S.; Motherwell, W. B.; Ozbalik, N.; Schwartzentruber, K. M. *J. Chem. Soc., Perkin Trans. 1* **1986**, 947$-$955.

(48) Ito, S.; Inoue, K.; Mastumoto, M. *J. Am. Chem. Soc.* **1982**, *104*, 6450$-$6452.

progress and will be reported in due course. Aspects of the present study have been published in a preliminary report.[49]

Experimental Section

Preparation of Compounds. All operations were performed under a pure dinitrogen or argon atmosphere using Schlenk techniques on an inert gas/vacuum manifold or in a drybox (O_2, H_2O < 1 ppm). Hexane, petroleum ether, and toluene were distilled over Na, and THF and diethyl ether over Na/Ph_2CO. Acetonitrile and methylene chloride were distilled over CaH_2. Ethanol and methanol were distilled over the corresponding magnesium alkoxide, and acetone over drierite. Anhydrous pyridine and dimethyl sulfoxide (water < 0.005%) and double-distilled acetic acid (metallic impurities in ppt) were purchased from Aldrich. All solvents, with the exception of methanol, were degassed by three freeze−pump−thaw cycles. Methanol and water were degassed by bubbling nitrogen or argon for 0.5 h. Compounds [Fe_3O(O_2CCH_3)_6(py)_3]·py (**1**)[50] and [Fe_2ZnO(O_2CCH_3)_6(py)_3]·py (**1''**)[51] were prepared according to literature procedures. Other starting materials were purchased from Aldrich and are of the highest available purities.

[Zn$_2$Fe^{II}(O$_2$CCH$_3$)$_6$(py)$_2$] (2). Zn powder (1.32 g, 0.02 mol) was added to a brown-black solution of [Fe_3O(O_2CCH_3)_6(py)_3]·py (**1**) (342 mg, 0.40 mmol) in 4.5 mL of acetonitrile and 0.45 mL of acetic acid. The reaction mixture was stirred for 0.5 h, and the excess Zn was filtered off. The light yellow supernatant afforded the pure product **2** (630 mg, 75% based on Fe) as light-yellow plates upon cooling (−20 °C). The same product can be obtained pure from the following reaction solvents: acetonitrile (3.0 mL)/acetic acid (1.5 mL); dichloromethane (4.5 mL)/acetic acid (0.45 mL); and pyridine (3.0 mL)/acetic acid (1.5 mL). In the last case, the pure product was obtained by slow diffusion of diethyl ether into the yellow-green supernatant at −20 °C (vide infra for an alternative method of preparation). ^{1}H NMR ((CD$_3$)$_2$SO, 0.98 × 10^{-2} M): δ 12.01 (s, br, 2-*H*-py), 8.54 (s, br, 3-*H*-py), 8.06 (t, $^3J_{HH}$ = 7.6 Hz, 4-*H*-py). IR (KBr): ν_{OCO} 1643, 1586, 1428, 1311 cm^{-1}. Near-IR/ATR (solid **2**): λ_{max} ≈ 980, 1260 nm. UV−vis (CH$_2$Cl$_2$): λ_{max} = 346 (ϵ_M = 209) nm. ^{57}Fe Mössbauer (4.2 K): δ 1.38 mm/s (ΔE_Q = 2.96 mm/s, Γ = 0.26 mm/s). Anal. Calcd for C$_{22}$H$_{28}$N$_2$Fe$_1$O$_{12}$Zn$_2$: C, 37.80; H, 4.04; N, 4.01; Fe, 7.99; Zn, 18.71. Found: C, 38.28; H, 4.12; N, 4.15; Fe, 8.18; Zn, 18.37.

[Fe^{II}(O$_2$CCH$_3$)$_2$(py)$_4$] (3). Zn powder (1.32 g, 0.02 mol) was added to a brown-black solution of **1** (342 mg, 0.40 mmol) in 4.5 mL of pyridine and 0.45 mL of acetic acid. The reaction mixture was stirred for 0.5 h, and the excess Zn was filtered off. Upon cooling (−20 °C), the yellow-green filtrate afforded the pure product as yellow-green polyhedra (489 mg, 83%). The same product was obtained pure from pyridine (4.0 mL)/acetic acid (0.8 mL) or neat pyridine (5.0 mL). In the latter case, the reaction was stirred for 6 h and the yellow-brown filtrate afforded **3** (459 mg, 78%) at −20 °C. Slow diffusion of diethyl ether into the supernatant precipitated a brown-black amorphous solid (70 mg) of unknown composition. The latter retains Fe(III) according to Mössbaur data. Preactivation of the Zn dust (washing with dilute HCl, acetic acid, and pyridine) eliminates the brown-black byproduct in the reduction (30 min) of **1** in pyridine.

Compound **3** was also obtained pure in the following manners. (i) A brown-black solution of **1** (342 mg, 0.40 mmol) in 5.0 mL of pyridine or pyridine (4.5 mL)/acetic acid (0.45 mL) was pressurized with dihydrogen (30 psig) over Pd (10 mg) for 2 h. After filtration of the catalyst, the clear yellow-green solution afforded **3** in quantitative yield upon cooling (−20 °C). (ii) Iron powder (1.3 g, 0.023 mol) was added to a brown-black solution of **1** (342 mg, 0.40 mmol) in 5.0 mL of pyridine or pyridine (4.5 mL)/acetic acid (0.45 mL). The reaction mixture was allowed to stir for 6 h (py) or 0.5 h (py/AcOH), followed by filtration of the excess Fe. Upon cooling (−20 °C), the bright yellow-green filtrate afforded **3** (471 mg, 80%). (iii) Iron powder (1.3 g, 0.023 mol) stirred for 0.5 h in pyridine (4.5 mL)/acetic acid (0.45 mL) afforded **3** (185 mg, 1.6%) from the filtrate at −20 °C. ^{1}H NMR ((CD$_3$)$_2$SO, 1.40 × 10^{-2} M): δ 72.43 (s, br, C*H*$_3$CO$_2$), 13.98 (s, br,

(49) Singh, B.; Long, J. R.; Papaefthymiou, G. C.; Stavropoulos, P. *J. Am. Chem. Soc.* **1996**, *118*, 5824−5825.

(50) Sorai, M.; Kaji, K.; Hendrickson, D. N.; Oh, S. M. *J. Am. Chem. Soc.* **1986**, *108*, 702−708.

(51) Blake, A. B.; Yavari, A.; Hatfield, W. E.; Sethulekshmi, C. N. *J. Chem. Soc., Dalton Trans.* **1985**, 2509−2520.

2-*H*-py), 9.01 (s, br, 3-*H*-py), 8.15 (t, $^3J_{HH}$ = 7.6 Hz, 4-*H*-py). IR (KBr): ν_{OCO} 1606, 1596, 1445, 1419 cm^{-1}. Near-IR/ATR (solid **3**): λ_{max} ≈ 860, 970 nm. UV−vis (py): λ_{max} = 396 (ϵ_M = 2107) nm. ^{57}Fe Mössbauer (4.2 K): δ 1.22 mm/s (ΔE_Q = 3.23 mm/s, Γ = 0.18 mm/s). Anal. Calcd for C$_{24}$H$_{26}$N$_4$Fe$_1$O$_4$: C, 58.79; H, 5.34; N, 11.43. Found: C, 58.68; H, 5.31; N, 11.37.

[Fe$^{II}_2$(O$_2$CCH$_3$)$_4$(py)$_3$]$_n$ (4). Compound **3** (300 mg, 0.61 mmol) was dissolved in 4.0 mL of pyridine. Diethyl ether (40 mL) was carefully added to the pyridine solution, with occasional shaking of the flask to disperse local clouding, until a small amount of a white solid, which would not easily redissolve, was apparent. The solution was filtered and diethyl ether was allowed to diffuse slowly into the filtrate at 10 °C. The product crystallized over a period of 1 week as large yellow polyhedra (115 mg, 64%) suitable for X-ray analysis. Rigorous exclusion of dioxygen is essential, for the product is exceedingly air-sensitive. Compound **4** was also obtained pure, but in a feathery form, from pyridine (4.0 mL)/acetic acid (0.8 mL) by diffusion of diethyl ether at 10 °C or from pyridine (3.0 mL)/acetic acid (1.5 mL) followed by diffusion of diethyl ether at −20 °C. ^{1}H NMR ((CD$_3$)$_2$SO, 1.23 × 10^{-2} M): δ 74.37 (s, br, C*H*$_3$CO$_2$), 12.62 (s, br, 2-*H*-py), 8.59 (s, br, 3-*H*-py), 8.04 (t, $^3J_{HH}$ = 7.6 Hz, 4-*H*-py,). IR (KBr): ν_{OCO} 1617, 1600, 1446, 1415 cm^{-1}. Near-IR/ATR (solid **4**): λ_{max} ≈ 850, 1100 nm. UV−vis (py, >1.0 × 10^{-3} M): λ_{max} = 424 (sh), 396 (ϵ_M = 2107, **3**) nm. ^{57}Fe Mössbauer (4.2 K): δ 1.27 mm/s (ΔE_Q = 2.92 mm/s, Γ = 0.20 mm/s). Anal. Calcd for C$_{23}$H$_{27}$N$_3$Fe$_2$O$_8$: C, 47.21; H, 4.65; N, 7.18. Found: C, 47.87; H, 4.97; N, 7.45.

[Zn(O$_2$CCH$_3$)$_2$(py)$_2$] (5). Diethyl ether was slowly diffused to a solution of Zn(O$_2$CCH$_3$)$_2$·2H$_2$O (439 mg, 2.0 mmol) in pyridine (20 mL) at −20 °C. Large colorless crystals of the product (crystal system: *tetragonal*) were deposited (574 mg, 84%). The same stoichiometric product was also obtained from py/AcOH solutions (10:1, 5:1) upon diffusion of diethyl ether. However, **5** obtained from py/AcOH(5:1)/Et$_2$O crystallizes in the *triclinic* crystal system (see also isolation of the product in reactivity studies). ^{1}H NMR ((CD$_3$)$_2$SO): 8.58 (d, 2H, $^3J_{HH}$ = 4.4 Hz, 2-*H*-py), 7.83 (tt, 1H, $^3J_{HH}$ = 7.6 Hz, 4-*H*-py), 7.43 (m, 2H, 3-*H*-py), 1.80 (s, 3H, C*H*$_3$CO$_2$). Anal. Calcd for C$_{14}$H$_{16}$N$_2$ZnO$_4$: C, 49.22; H, 4.72; N, 8.20. Found: C, 48.59; H, 4.60; N, 7.98.

[Zn$_2$(O$_2$CCH$_3$)$_4$(py)$_2$] (6). Diethyl ether was slowly diffused to a solution of **5** (342 mg, 1.0 mmol) in 10 mL of pyridine and 5 mL of acetic acid at −20 °C. Large colorless plates of the product (crystal system: *monoclinic*) were deposited (200 mg, 76%) (see also isolation of the product in reactivity studies). ^{1}H NMR ((CD$_3$)$_2$SO): 8.58 (br, 2H, 2-*H*-py), 7.81 (tt, 1H, $^3J_{HH}$ = 7.8 Hz, 4-*H*-py), 7.41 (m, 2H, 3-*H*-py), 1.79 (s, 6H, C*H*$_3$CO$_2$). Anal. Calcd for C$_{18}$H$_{22}$N$_2$Zn$_2$O$_8$: C, 41.17; H, 4.22; N, 5.33. Found: C, 41.04; H, 4.13; N, 5.17.

[Zn(O$_2$CCH$_3$)$_2$(py)]$_n$ (7). A solution of **5** (342 mg, 1.0 mmol) in ethanol (20 mL) or dichloromethane (20 mL) was evaporated to a small volume until colorless plates were apparent. The product was redissolved in situ upon mild heating and allowed to crystallize slowly (189 mg, 72%) at −20 °C. ^{1}H NMR (CD$_3$CD$_2$OD): 8.57 (d, 2H, $^3J_{HH}$ = 6.4 Hz, 2-*H*-py), 7.91 (tt, 1H, $^3J_{HH}$ = 7.8 Hz, 4-*H*-py), 7.49 (m, 2H, 3-*H*-py), 1.95 (s, 6H, C*H*$_3$CO$_2$). Anal. Calcd for C$_9$H$_{11}$NZnO$_4$: C, 41.17; H, 4.22; N, 5.33. Found: C, 41.10; H, 4.10; N, 5.26.

[Zn$_3$(O$_2$CCH$_3$)$_6$(py)$_2$] (8). A solution of **5** (342 mg, 1.0 mmol) in acetonitrile (20 mL) was evaporated until colorless crystals were apparent. The product was redissolved in situ upon mild heating and allowed to crystallize slowly (203 mg, 86%) at −20 °C. The product was also obtained by recrystallization of **6** (525 mg, 1.0 mmol) in dichloromethane (5 mL). ^{1}H NMR (CD$_2$Cl$_2$): 8.63 (dd, 2H, $^3J_{HH}$ = 6.0 Hz, 2-*H*-py), 7.87 (tt, 1H, $^3J_{HH}$ = 7.6 Hz, 4-*H*-py), 7.45 (t, 2H, $^3J_{HH}$ = 6.8 Hz, 3-*H*-py), 2.06 (s, 9H, C*H*$_3$CO$_2$). Anal. Calcd for C$_{22}$H$_{28}$N$_2$O$_{12}$Zn$_3$: C, 37.29; H, 3.98; N, 3.95. Found: C, 37.32; H, 3.89; N, 4.06.

[PPN][Fe^{II}(O$_2$CCH$_3$)$_3$(py)] (9). Compound **3** (300 mg, 0.61 mmol) and [PPN][O$_2$CCH$_3$] (360 mg, 0.60 mmol) were dissolved in 5.0 mL of pyridine upon stirring. The yellow-orange solution was filtered and diethyl ether was allowed to diffuse slowly into the filtrate at 20 °C. The yellow product crystallized as long needles (237 mg, 46%). ^{1}H NMR ((CD$_3$)$_2$SO): δ 67.64 (br, C*H*$_3$CO$_2$), 9.56 (s, br, 2-*H*-py), 7.85 (t, $^3J_{HH}$ = 7.6 Hz, 4-*H*-py), 7.69 (t, $^3J_{HH}$ = 7.0 Hz, 3-*H*-py), 7.53−7.60 (m, P*Ph*$_3$). IR (KBr): ν_{OCO} 1604, 1590, 1440 cm^{-1}. UV−vis (py): λ_{max} = 396 (**3**), 342 (ϵ_M = 192) nm. ^{57}Fe Mössbauer (4.0 K): δ 1.21

mm/s (ΔE_Q = 2.97 mm/s, Γ = 0.25 mm/s). Anal. Calcd for $C_{47}H_{44}N_1Fe_1O_6P_2$: C, 66.36; H, 5.21; N, 3.29; P, 7.28. Found: C, 66.15; H, 5.08; N, 3.15; P, 7.11.

[Fe^{II}(H$_2$O)$_4$(py)$_2$][O$_2$CCH$_3$]$_2$ (10). Compound **3** (300 mg, 0.61 mmol) was dissolved in 5.0 mL of pyridine upon stirring. To the yellow-green solution was added 0.5 mL of water, and diethyl ether was allowed to diffuse slowly into the filtrate at 20 °C. The product deposited as light-yellow crystals (122 mg, 49%). ^{1}H NMR ((CD$_3$)$_2$-SO): δ 54.79 (br, CH_3CO$_2$), 13.20 (s, 4H, 2-*H*-py), 8.90 (m, 4H, 3-*H*-py), 8.11 (t, 2H, $^3J_{HH}$ = 8.0 Hz, 4-*H*-py), 3.57 (s, 8H, H_2O). IR (KBr): ν_{OCO} 1617, 1600, 1420 cm^{-1}. UV−vis (py): λ_{max} = 396 (**3**) (ϵ_M = 1958) nm. ^{57}Fe Mössbauer (4.2 K): δ 1.28 mm/s (ΔE_Q = 3.00 mm/s, Γ = 0.15 mm/s). Anal. Calcd for $C_{14}H_{24}N_2Fe_1O_8$: C, 41.60; H, 5.98; N, 6.93. Found: C, 41.67; H, 5.84; N, 6.30.

[Fe^{III}$_3$(O$_2$CCH$_3$)$_6$(OS(CH$_3$)$_2$)$_2$]$_n$ (11). Compound **3** (10 mg, 0.02 mmol) which was allowed to stand in dimethyl sulfoxide-d_6 (0.5 mL) for 48 h, deposited colorless crystals of the deuterated title compound. On a preparative scale, compound **11** can be synthesized by dissolving [Fe^{II}(O$_2$CCH$_3$)$_2$] (100 mg, 0.57 mmol) in dimethyl sulfoxide (40 mL), followed by filtration and diffusion of diethyl ether into the filtrate (20 °C) to yield colorless plates of the product. ^{1}H NMR ((CD$_3$)$_2$SO, 7.37 × 10^{-3} M): δ 62.22 (br, CH_3CO$_2$), 2.53 (br, (CH_3)$_2$SO). IR (KBr): ν_{OCO} 1507, 1437, 1419 cm^{-1}. UV−vis ((CH$_3$)$_2$SO): λ_{max} = 270 (ϵ_M = 167) nm. ^{57}Fe Mössbauer (4.2 K): δ 1.40 mm/s (ΔE_{Q1} = 3.04 mm/s, Γ_1 = 0.20 mm/s, 66%); 1.38 mm/s (ΔE_{Q2} = 2.94 mm/s, Γ_2 = 0.22 mm/s, 34%). Anal. Calcd for $C_{16}H_{30}Fe_3O_{14}S_2$: C, 28.34; H, 4.46; S, 9.46. Found: C, 28.43; H, 4.71; S, 9.37.

Reaction of Ferrous Species with Dioxygen. The following compounds were isolated during investigations directed toward the elucidation of the reactivity of ferrous species with dioxygen.

[Fe$_3$O(O$_2$CCH$_3$)$_6$(py)$_3$]·py (1). Dioxygen was admitted to a solution of compound **3** (300 mg, 0.61 mmol) in pyridine (20 mL) at −20 °C for 4 h. The solution was filtered, and the brown filtrate was reduced under vacuum to 10 mL. Diffusion of diethyl ether into the filtrate at −20 °C afforded brown-black blocks of the product (150 mg, 86%). Pyridine/acetic acid (10:1 v/v) was also used as the reaction solvent with identical results. The product was identified by crystallographic unit cell parameters and ^{1}H NMR by comparison with an authentic sample and literature citations.[50]

[Fe$_{2.22(2)}$Zn$_{0.78(2)}$O(O$_2$CCH$_3$)$_6$(py)$_3$]·py (1′). [Zn$_2$Fe^{II}(O$_2$CCH$_3$)$_6$(py)$_2$] (**2**) (350 mg, 0.50 mmol) was dissolved in 27 mL of pyridine and 2.7 mL of acetic acid and allowed to react with 1 atm of pure dioxygen or simply air for 2 h. A brown-black solution was rapidly generated—a short induction period was observed with pure dioxygen—from which, after reduction of the solvent to 10 mL (solvent composition after evaporation: py:AcOH 2:1 v/v) and diffusion of diethyl ether at −20 °C, the brown-black crystalline product **1′** was obtained (185 mg, 95% based on Fe). ^{1}H NMR ((CD$_3$)$_2$SO): δ 31.37 (s, br, CH_3CO$_2$), 13.03 (s, br, CH_3CO$_2$), 8.58 (s, br, 2-H-py), 7.78 (t, $^3J_{HH}$ = 8.0 Hz, 4-H-py), 7.40 (s, br, 3-H-py). IR (KBr): ν_{OCO} 1631, 1614, 1447, 1412 cm^{-1}. UV−vis (py): λ_{max} 470 (ϵ_M = 431), 352 (ϵ_M = 3170), 320 (ϵ_M = 3150) nm. ^{57}Fe Mössbauer (20 K): δ_1 0.53 mm/s (ΔE_{Q1} = 1.15 mm/s, Γ_1 = 0.21 mm/s, 90%), δ_2 1.25 mm/s (ΔE_{Q2} = 2.11 mm/s, Γ_2 = 0.20 mm/s, 10%). Anal. Calcd for $C_{32}H_{38}N_4Fe_{2.2}O_{13}Zn_{0.78}$: C, 44.61; H, 4.45; N, 6.50; Fe, 14.39; Zn, 5.92. Found (analyses on two independently prepared samples were obtained): C, 44.57 (44.26); H, 4.38 (4.46); N, 6.45 (6.27); Fe, 14.38 (14.13); Zn, 5.80 (6.08).

Diffusion of diethyl ether into the remaining supernatant of **1′** afforded colorless polyhedra (crystal system: *orthorhombic*) of [Zn$_2$(O$_2$-CCH$_3$)$_4$(py)$_2$] (**6**) (197 mg, 75% based on Zn) (vide supra for analytical details).

[Fe$_2$ZnO(O$_2$CCH$_3$)$_6$(py)$_3$]·py (1″). Zn powder (1.32 g, 0.02 mol) was added to a solution of compound **1** (342 mg, 0.40 mmol) in pyridine (20 mL), and the reaction mixture was vigorously stirred for 6 h. To the yellow-brown filtrate (which affords compound **3** if allowed to cool at −20 °C) was admitted dioxygen for 2 h at ambient temperature. The product was obtained as large red−green dichroic crystals (220 mg, 42% based on Fe in **1**) upon diffusion of diethyl ether at −20 °C into the resulting brown-black solution after oxygenation. The product was characterized by analytical and ^{1}H NMR data by comparison with an authentic sample and literature citations, but it crystallized in a *monoclinic* rather than the reported[51] *rhombohedral* space group. Anal.

Calcd for $C_{32}H_{38}N_4Fe_2O_{13}Zn_1$: C, 44.50; H, 4.43; N, 6.49; Fe, 12.93; Zn, 7.57. Found: C, 44.32; H, 4.48; N, 6.41; Fe, 12.84; Zn, 7.51.

Equilibrium-Dependent Transformations. Interconversions among species **2**−**5** were observed under the following conditions.

[Zn$_2$Fe^{II}(O$_2$CCH$_3$)$_6$(py)$_2$] (2) in Pyridine. Compound **2** (350 mg, 0.50 mmol) was dissolved in 4.0 mL of pyridine to yield a yellow-green solution, from which large yellow-green crystals of [Fe^{II}(O$_2$-CCH$_3$)$_2$(py)$_4$] (**3**) (226 mg, 92%) were obtained upon cooling (−20 °C). Diffusion of diethyl ether into the supernatant afforded colorless plates (crystal system: *tetragonal*) of [Zn(O$_2$CCH$_3$)$_2$(py)$_2$] (**5**) (325 mg, 95%). The same result is obtained in py/AcOH (10:1).

Regeneration of [Zn$_2$Fe^{II}(O$_2$CCH$_3$)$_6$(py)$_2$] (2) from Compounds 3 and 5. Compound **2** (321 mg, 92%) was obtained by mixing [Fe^{II}(O$_2$-CCH$_3$)$_2$(py)$_4$] (**3**) (245 mg, 0.50 mmol) and [Zn(O$_2$CCH$_3$)$_2$(py)$_2$] (**5**) (342 mg, 1.0 mmol) in pyridine (5.0 mL) or pyridine (3.0 mL)/acetic acid (1.5 mL), followed by careful addition of a layer of diethyl ether (50 mL) and allowing the solution to stand at 10 °C. Dichloromethane (5.0 mL), acetonitrile (5.0 mL), and dimethyl sulfoxide (5.0 mL) were also used as reaction solvents, affording essentially quantitative yields of **2**.

Catalytic Oxidations. A typical oxidation of substrate (adamantane) mediated by iron-containing species (for instance, compound **1**) was performed as follows. Compound **1** (30.0 mg, 35.1 μmol) was dissolved under anaerobic conditions in 27 mL of pyridine and 2.7 mL of acetic acid followed by adamantane (100 mg, 0.73 mmol). Zn powder (1.3 g, 99.998%) was added to this solution, and the mixture was stirred for 18 h under pure dioxygen (delivered to the head space of the oxygen-saturated solution under static conditions) or simply open to air. The internal standard (hexamethylbenzene) was added to the mixture, and an aliquot (2 mL) was withdrawn for GC or GC−MS analysis. After addition of water (3 mL), the aliquot was extracted with diethyl ether (3 × 5 mL). The combined diethyl ether layers were washed with water and dried over magnesium sulfate. The samples were analyzed by a Perkin-Elmer SIGMA 2000 or a Hewlett-Packard 5890 Series II Capillary GC employing Supelco SPB-1, SPB-50, and SUPELCO-WAX-10 (adamantane oxidation) capillary columns (30 m (length), 0.32 mm (i.d.), 0.25 μm (d_f)), a flame ionization detector, and a Hewlett-Packard 3395 or 3396A integrator. Products were identified by their respective retention times versus authentic samples and by mass determination on a Finnigan MAT-90 MS coupled to a Varian 3400 GC.

In the catalytic oxidation of benzene, toluene, and *cis*-stilbene, the molar ratio of substrate over catalyst was also kept at 20:1. In contrast, a large excess of isopentane (17.19 mmol) was employed. Static delivery of dioxygen in a closed system was performed in the case of the volatile isopentane, benzene, and toluene. Quantification of hydroxypyridines, produced in the catalytic oxidation of pyridine, was performed by ^{1}H NMR in (CD$_3$)$_2$CO/D$_2$O following a reported protocol.[29]

Kinetic Isotope Effect Measurements. The intermolecular deuterium kinetic isotope effect was measured for adamantane by conducting catalytic oxidations (as previously described, but maintained at 25.0(1) °C with the aid of a Brinkmann RM6 thermostat) on a mixture of adamantane/adamantane-d_{16} (1:1). KIE values were calculated for each product (average of three trials) from the ratio of protio/deuterio product yield, measured by GC analysis and GC−MS calculation of the relative intensities of the respective molecular ions selected over the fully resolved GC peaks. Corrections for the exact adamantane/adamantane-d_{16} ratio used, as determined by GC−MS, were applied.

X-ray Structure Determinations. Structures were determined for the compounds listed in Tables 1 and 2. Single crystals were picked from the reaction products, sealed in capillaries under an inert atmosphere and/or coated with Paratone-N oil, and transferred to a Siemens SMART (**9**) or a Nicolet P3 (all others) diffractometer. Lattice parameters were obtained from a least-squares analysis of more than 30 carefully centered reflections. None of the crystals showed significant decay during data collection. The raw intensity data were converted (including corrections for scan speed, background, and Lorentz and polarization effects) to structure factor amplitudes and their esd's. An empirical absorption correction based on the observed variation in intensity of azimuthal (Ψ) scans was applied to the data sets for compounds **7**, **9**, and **11**.

Table 1. Crystallographic Data[a] for [Fe$_{2.22(2)}$Zn$_{0.78(2)}$O(O$_2$CCH$_3$)$_6$(py)$_3$]·py (**1′**), [Fe$_2$ZnO(O$_2$CCH$_3$)$_6$(py)$_3$]·py (**1″**), [Zn$_2$Fe^{II}(O$_2$CCH$_3$)$_6$(py)$_2$] (**2**), [Fe^{II}(O$_2$CCH$_3$)$_2$(py)$_4$] (**3**), [Fe$^{II}_2$(O$_2$CCH$_3$)$_4$(py)$_3$]$_n$ (**4**), and [Zn(O$_2$CCH$_3$)$_2$(py)$_2$] (**5**)

	1′	1″	2	3	4	5	5
formula	C$_{32}$H$_{38}$Fe$_{2.22}$N$_4$O$_{13}$Zn$_{0.78}$	C$_{32}$H$_{38}$Fe$_2$N$_4$O$_{13}$Zn	C$_{22}$H$_{28}$FeN$_2$O$_{12}$Zn$_2$	C$_{24}$H$_{26}$FeN$_4$O$_4$	C$_{23}$H$_{27}$Fe$_2$N$_3$O$_8$	C$_{14}$H$_{16}$N$_2$O$_4$Zn	C$_{14}$H$_{16}$N$_2$O$_4$Zn
formula wt	861.66	863.76	699.10	490.34	585.18	341.66	341.66
cryst syst	trigonal	monoclinic	monoclinic	orthorhombic	orthorhombic	tetragonal	triclinic
space group	$R32$	$C2$	$P2_1/n$	$Pccn$	$Pna2_1$	$P4_32_12$	$P\bar{1}$
Z	3	2	2	4	4	4	2
a, Å	17.556(4)	12.553(2)	10.255(2)	8.857(7)	16.018(4)	8.613(2)	8.370(2)
b, Å		17.574(3)	10.756(2)	16.401(9)	9.687(3)		9.021(2)
c, Å	10.932(5)	10.825(2)	12.727(3)	16.653(10)	18.107(6)	22.534(5)	10.998(2)
α, deg							93.57 (1)
β, deg		124.00(2)	95.56(3)				102.32(1)
γ, deg							95.38(1)
V, Å^3	2918(2)	1979.7(5)	1397.2(5)	2419(3)	2810(1)	1671.6(6)	804.8(3)
T, K	223	295	223	223	295		
color	red-black	red−green dichroic	light yellow	yellow-green	yellow	colorless	colorless
d_{calc}, g/cm^3	1.469	1.513	1.662	1.346	1.383	1.358	1.410
μ, mm^{-1}	1.329	1.398	2.277	0.660	1.079	1.484	1.541
R^b ($R_w{}^c$ or $wR_2{}^d$), %	4.16 (4.61)^c	4.13 (4.21)^c	3.34 (3.62)^c	3.91 (3.83)^c	3.88 (8.87)^d	3.62 (3.91)^d	3.25 (8.70)^d

[a] Obtained with graphite monochromated Mo Kα (λ = 0.710 73 Å) radiation. [b] $R = \sum||F_o| - |F_c||/\sum|F_o|$. [c] $R_w = \{\sum[w(|F_o| - |F_c|)^2/\{\sum[w|F_o|^2]\}^{1/2}$. [d] $wR_2 = \{\sum[w(F_o{}^2 - F_c{}^2)^2/\{\sum[w(F_o{}^2)^2]\}^{1/2}$.

Table 2. Crystallographic Data[a] for [Zn$_2$(O$_2$CCH$_3$)$_4$(py)$_2$] (**6**), [Zn(O$_2$CCH$_3$)$_2$(py)]$_n$ (**7**), [Zn$_3$(O$_2$CCH$_3$)$_6$(py)$_2$] (**8**), [PPN][Fe^{II}(O$_2$CCH$_3$)$_3$(py)] (**9**), [Fe^{II}(H$_2$O)$_4$(*trans*-py)$_2$][O$_2$CCH$_3$]$_2$ (**10**), and [Fe$^{III}_3$(O$_2$CCH$_3$)$_6$((OS(CD$_3$)$_2$)$_2$]$_n$ (**11**)

	6	6	7	8	9	10	11
formula	C$_{18}$H$_{22}$N$_2$O$_8$Zn$_2$	C$_{18}$H$_{22}$N$_2$O$_8$Zn$_2$	C$_9$H$_{11}$NO$_4$Zn	C$_{22}$H$_{28}$N$_2$O$_{12}$Zn$_3$	C$_{47}$H$_{44}$FeN$_2$O$_6$P$_2$	C$_{14}$H$_{24}$FeN$_2$O$_8$	C$_{16}$H$_{18}$D$_{12}$Fe$_3$O$_{14}$S$_2$
formula wt	525.12	525.12	262.58	708.64	850.67	404.20	690.15
cryst syst	orthorhombic	monoclinic	triclinic	monoclinic	monoclinic	triclinic	monoclinic
space group	$Pbca$	$C2/c$	$P\bar{1}$	$P2_1/n$	$P2_1/n$	$P\bar{1}$	$C2$
Z	4	4	8	2	4	1	2
a, Å	13.182(3)	9.940(1)	8.626(2)	10.306(2)	9.1187(3)	7.999(2)	12.679(2)
b, Å	8.601(2)	17.259(2)	8.868(3)	10.837(3)	14.6294(4)	8.002(2)	12.483(2)
c, Å	19.485(6)	12.620(2)	28.871(8)	12.647(4)	32.8906(5)	8.401(2)	8.518(1)
α, deg			90.17(2)			69.79(2)	
β, deg		97.26(1)	90.02(2)	95.16(2)	92.56(0)	69.69(2)	94.76(1)
γ, deg			99.02(2)			74.94(2)	
V, Å^3	2209(1)	2147.7(5)	2181(1)	1406.7(6)	4383.3(2)	467.3(2)	1343.5(4)
color	colorless	colorless	colorless	colorless	yellow	yellow	colorless
d_{calc}, g/cm^3	1.579	1.624	1.599	1.673	1.289	1.436	1.68
μ, mm^{-1}	2.216	2.280	2.245	2.599	0.467	0.849	1.82
R (R_w or wR_2),^{b} %	4.71 (4.63)^c	5.17 (12.57)^d	5.42 (5.96)^c	3.51 (3.81)^c	6.06 (10.62)^c	4.37 (11.00)^c	3.75 (7.37)^c

[a] Obtained at 295 with graphite monochromated Mo Kα (λ = 0.710 73 Å) radiation. [b] For definitions cf. Table 1. [c] R_w. [d] wR_2.

Space group assignments were based on systematic absences, E statistics, and successful refinement of the structures. Structures were solved by direct methods with the aid of successive difference Fourier maps and refined using either the SHELXTL PLUS 4.21/V or the SHELXTL 5.0 software package. Thermal parameters for all non-hydrogen atoms were refined anisotropically. In the structures of compounds **1″**, **5** (tetragonal), **6** (orthorhombic), **7**, and **8**, hydrogen atoms were fixed at ideal locations 0.96 Å from the bonded carbon atom and given a uniform value of U_{iso}. In the structure of **9**, all hydrogen atoms were located from difference Fourier maps and refined with isotropic thermal parameters. For all other structures, hydrogen atoms were assigned to ideal positions and refined using a riding model with an isotropic thermal parameter 1.2 times that of the attached carbon atom (1.5 times for methyl hydrogens). In the structure of **1″**, the iron and zinc atoms could not be differentiated and were evenly distributed over the two metal sites; the carbon and nitrogen atoms in its pyridine solvate molecule were treated similarly. Hydrogen atoms were not included for this disordered pyridine. Crystallographic data are listed in Tables 1 and 2. Further details of the structure determinations are deposited as Supporting Information.

Magnetic Measurements. Magnetic susceptibilities for the one-dimensional chain compounds **4** and **11** were obtained on a Quantum Design AC MRMS-5S SQUID magnetosusceptometer equipped with a 5.5 T magnet. Data were collected in the temperature range 2−300 K (total of 95 temperature points) at a field strength of 0.2 T and were corrected for the magnetization of the sample holder and for diamagnetic contributions as estimated from Pascal constants[52] (χ_{dia} = −353 × 10^{-6} emu mol^{-1} for **4** and −312 × 10^{-6} emu mol^{-1} for **11**).

Other Physical Measurements. ^{1}H and ^{13}C NMR spectra were recorded on Varian XL-400 and JEOL GSX-270 NMR spectrometers. The isotropically shifted peaks for the iron-containing compounds were assigned on the basis of chemical shift, integration, and selective deuteration. FT-IR spectra were obtained on a Perkin-Elmer 1800 FT-IR spectrometer. FT-near-IR spectra were recorded on a Bruker Vector 22 FT-near-IR spectrometer (Ge or InAs detectors) equipped with a fiber optic sample probe for near-IR/ATR spectra of solids. UV−vis spectra were obtained on a Hewlett-Packard 8452A diode array spectrophotometer. Mössbauer data were recorded with a conventional Mössbauer spectrometer (^{57}Co source in a Rh matrix) operating at the constant acceleration mode and calibrated using a thin iron foil. Isomer shifts are reported relative to metallic iron at room temperature. SEM microprobe analysis was performed on a Kevex (Delta Series) energy dispersive X-ray spectrometer. Electrospray mass spectra were recorded using a Platform II MS (Micromass Instruments, Danvers, MA). Samples were introduced from py/AcOH (10:1) solutions at a flow rate of 5 μL/min from a syringe pump (Harvard Apparatus). The electrospray probe capillary was maintained at a potential of 3.0 kV, and the orifice to skimmer potential ("cone voltage") was varied from 15−30 V. Spectra were collected in the multichannel acquisition mode. EI and CI mass spectra were obtained on a Finnigan MAT-90 mass spectrometer. Microanalyses were done by H. Kolbe, Mikroanalytisches Laboratorium, Mülheim an der Ruhr, Germany.

(52) O'Connor, C. J. *Prog. Inorg. Chem.* **1982**, *29*, 203−283.
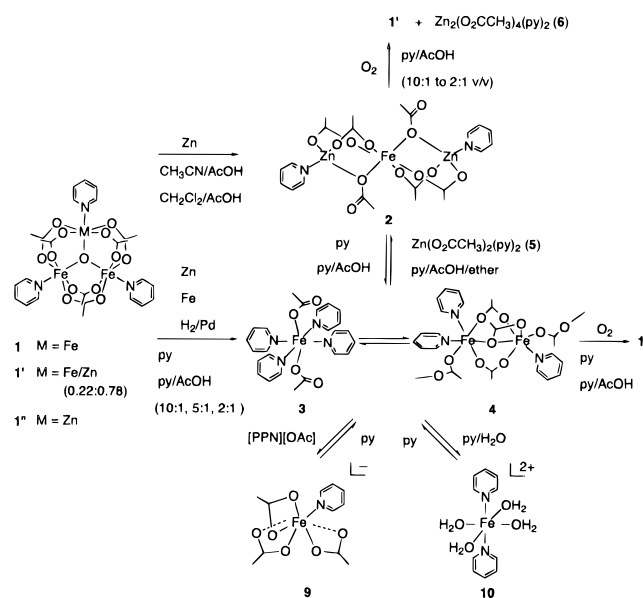
Scheme 1

Results and Discussion

Reduction of Basic Iron/Zinc Acetates. With reference to Scheme 1, reduction of brown-black $[Fe_3O(O_2CCH_3)_6(py)_3]\cdot$-py $(\mathbf{1})^{50}$ or dichroic red−green $[Fe_2ZnO(O_2CCH_3)_6(py)_3]\cdot py$ $(\mathbf{1''})^{51}$ with excess Zn in $CH_3CN/AcOH$ (10:1 or 2:1 v/v) or $CH_2Cl_2/AcOH$ (10:1), followed by Zn filtration, results in the precipitation of light yellow crystals of the air-sensitive compound $[Zn_2Fe^{II}(O_2CCH_3)_6(py)_2]$ (**2**), upon cooling (−20 °C). The analogous reduction (0.5 h) of **1** (or **1''**) with Zn in py/AcOH (10:1 or 5:1) affords yellow-green crystals of $[Fe^{II}(O_2\text{-}CCH_3)_2(py)_4]$ (**3**)^{53} directly from the reaction mixture at −20 °C. Evident in this reaction is the slow evolution of dihydrogen owing to the reaction of Zn with acetic acid. Prolonged interaction of **1** (or **1''**) with Zn is avoided, since products of solubilized Zn(OAc)$_2$ (vide infra) are accumulating and finally depositing from the reaction mixture. If diffusion of diethyl ether (Et$_2$O) into the py/AcOH filtrates of the reduction of **1** (or **1''**) with Zn is attempted at 10 °C, yellow crystals of $[Fe^{II}_2(O_2CCH_3)_4(py)_3]_n$ (**4**) are preferentially obtained. Depending on the constitution of the reaction mixture, these can be contaminated with **3** (py/AcOH 10:1), **2** (py/AcOH 5:1), and occasionally large colorless crystals of $[Zn(O_2CCH_3)_2(py)_2]$ (**5**).^{54} Direct addition, rather than diffusion, of a large excess of Et$_2$O to the py/AcOH reaction filtrates favors precipitation of **2**. Pure **2** is also consistently obtained by diffusion of Et$_2$O into the filtrate of the reduction of **1** with Zn in py/AcOH (2:1). Colorless $[Zn_2(O_2CCH_3)_4(py)_2]$ (**6**) is additionally isolated from py/AcOH (2:1) upon prolonged (>2 h) reduction of **1** (or **1''**) with Zn.

The inefficiency of catalytic Gif-type systems in pure pyridine prompted us to examine the reduction of **1** with excess Zn in the absence of AcOH. Prolonged (6 h) reduction results in a yellow-brown solution, from which compound **3** (80%) is

(53) This species has been previously reported but aspects of its synthesis and/or characterization have remained unclear: (a) Catterick, J.; Thornton, P.; Fitzsimmons, B. W. *J. Chem. Soc., Dalton Trans.* **1977**, 1420−1425. (b) Hardt, H.-D.; Möller, W. *Z. Anorg. Allg. Chem.* **1961**, *313*, 57−69. (c) Sheu, C.; Richert, S. A.; Cofré, Ross, B., Jr.; Sobkowiak, A.; Sawyer, D. T.; Kanofsky, J. R. *J. Am. Chem. Soc.* **1990**, *112*, 1936−1942.

(54) Solvation adducts of stoichiometry Zn(OAc)$_2$·2py along with some crystallographic data have been reported: (a) Bernard, M. A.; Busnot, A.; Busnot, F. *Bull. Soc. Chim. Fr.* **1970**, 2867−2870. (b) Bernard, M. A.; Busnot, A.; Busnot, F. *Bull. Soc. Chim. Fr.* **1971**, 1278−1282. (c) Bernard, M. A.; Busnot, F. *Bull. Soc. Chim. Fr.* **1972**, 3045−3051. (d) Semenenko, K. N.; Kurdyumov, G. M. *Vestn. Mosk. Univ., Ser. Mat., Mekh., Astron., Fiz., Khim.* **1958**, *13*, 207−209.

obtained at −20 °C. From the supernatant, a small amount of a brown-black film precipitates upon diffusion of Et$_2$O. Attempts to crystallize this material from organic solvents have been unsuccessful. Mössbauer data suggest that this species retains Fe(III), the amount of which is not diminished upon longer reaction times. However, employment of preactivated Zn dust (washed with HCl, CH$_3$COOH, and pyridine) enables complete and rapid (0.5 h) reduction to yellow-green solutions from which the aforementioned Fe(II) species are obtained.

Pyridine-Dependent Equilibria. The pattern of isolation of the different species, which at first appeared erratic, suggests that multiple equilibria may be operative. These potentially include monomer/dimer equilibria for both iron and zinc species independently, as well as heterometallic cross-coupling equilibria (eqs 16−18).

$$2n[Fe^{II}(O_2CCH_3)_2(py)_4] \; (\mathbf{3}) \rightleftharpoons$$
$$[Fe^{II}_2(O_2CCH_3)_4(py)_3]_n \; (\mathbf{4}) + (5n)py \quad (16)$$

$$[Fe^{II}(O_2CCH_3)_2(py)_4] \; (\mathbf{3}) + 2[Zn(O_2CCH_3)_2(py)_2] \; (\mathbf{5}) \rightleftharpoons$$
$$[Zn_2Fe^{II}(O_2CCH_3)_6(py)_2] \; (\mathbf{2}) + 6py \quad (17)$$

$$2[Zn(O_2CCH_3)_2(py)_2] \; (\mathbf{5}) \rightleftharpoons$$
$$[Zn_2(O_2CCH_3)_4(py)_2] \; (\mathbf{6}) + 2py \quad (18)$$
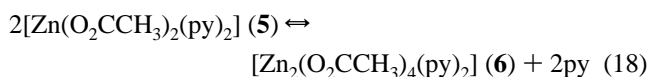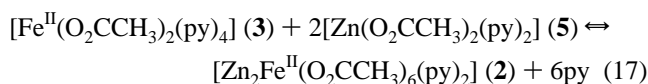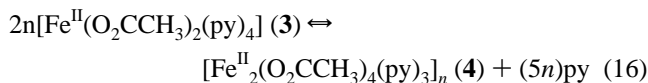
In agreement with this interpretation, dilution of pyridine solutions with AcOH/Et$_2$O or use of nonpyridine solvents in isolation procedures promotes an equilibrium shift in the direction $\mathbf{3} \rightarrow \mathbf{4}$ and $\mathbf{3(4)} + \mathbf{5} \rightarrow \mathbf{2}$. Further confirmation of the proposed equilibria is provided by the following control experiments which also serve as preparative methods. Compound **4** is obtained pure in the form of feathery crystals from saturated solutions of **3** in py/AcOH (5:1, 2:1) upon direct addition or diffusion of Et$_2$O. However, crystals of **4** suitable for X-ray analysis (vide infra) could only be prepared from concentrated solutions of **3** in neat pyridine upon fast addition of Et$_2$O (in order to avoid precipitation of **3**) and subsequent slow diffusion of Et$_2$O at 10 °C. Storage of the crystallization apparatus at lower temperatures favors precipitation of **3**. Supersaturated solutions of **3** in pyridine at room-temperature deposit **4** as a yellow powder, although the latter is frequently contaminated with **3**. Conversely, pure **4** when dissolved in pyridine or py/AcOH generates intense yellow-green solutions, from which **3** precipitates upon cooling (−20 °C).

In Gif-type solutions, equilibrium 17 lies predominantly on the left side. When dissolved in pyridine or py/AcOH (10:1, 5:1), light-yellow **2** affords intensely colored yellow-green solutions, from which essentially quantitative amounts of **3** and **5** are isolated upon cooling at −20 °C. Conversely, compound **3** and a 2-fold excess of **5** dissolved in pyridine or py/AcOH deposit light-yellow crystals of **2** *upon addition of excess Et$_2$O*. In a similar fashion, **2** is recovered quantitatively from solutions containing both **3** and **5** in CH$_3$CN, CH$_2$Cl$_2$, or DMSO.

Corroborative evidence for the pyridine-dependent equilibria among species **2**−**4** is provided by UV−vis spectra. Compound **3** demonstrates a characteristic charge-transfer absorption (λ_{max} 396 nm ($\epsilon_M = 2107$) in py; λ_{max} 388 nm ($\epsilon_M = 2084$) in py/AcOH (10:1); λ_{max} 368 nm ($\epsilon_M = 1900$) in py/AcOH (2:1)) in the concentration range 10^{-5}−10^{-4} M (Beer's law observed; Figure 2 (top)). At higher concentrations ($>1.0 \times 10^{-3}$ M in py; $>0.88 \times 10^{-3}$ M in py/AcOH (10:1); $>0.8 \times 10^{-3}$ M in py/AcOH (2:1)), a new broad absorption appears (λ_{max} 424 nm in py; λ_{max} 406 nm in py/AcOH (10:1); λ_{max} 400 nm in py/AcOH (2:1)) and Beer's law is no longer obeyed. At such high concentrations, the UV−vis criterion alone is not reliable
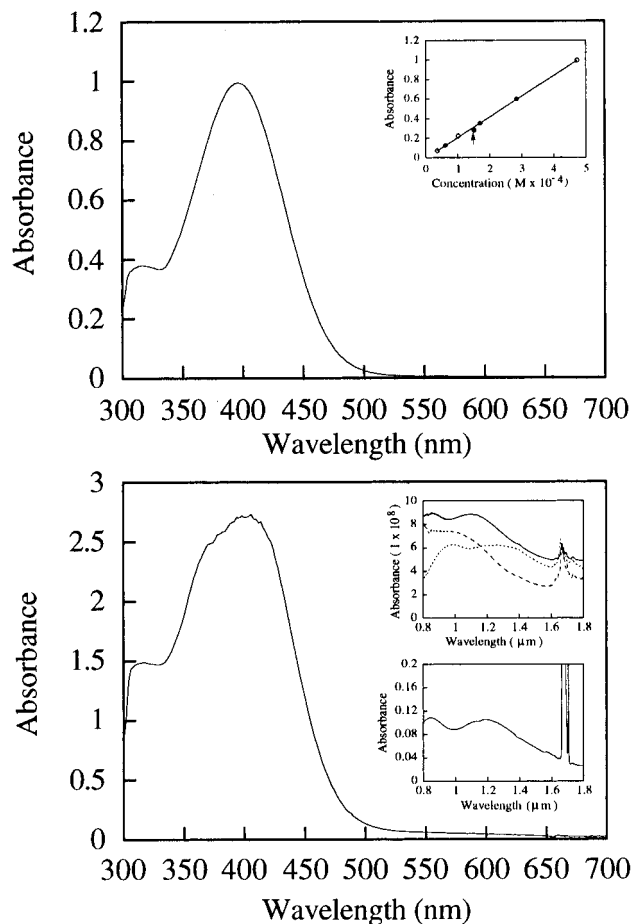
Figure 2. (top) Optical spectrum of **3** (4.73×10^{-4} M) in pyridine. The inset shows the absorbance at 396 nm as a function of concentration. The arrow pinpoints to a solution of **2** (1.51×10^{-4} M) in pyridine. (bottom) Optical spectrum of **3** (1.86×10^{-3} M) in pyridine. The top inset shows the near-IR spectra of solid **2** (dotted line), **3** (dashed line), and **4** (solid line). The bottom inset shows the near-IR spectrum of a solution of **3** (1.02×10^{-2} M) in py/AcOH (10:1).

evidence for the generation of new species in solution. However, in the near-IR region, solutions of **3** (10^{-3}–10^{-1} M) or equimolar filtrates of the reduction of **1** by Zn powder in py or py/AcOH (10:1, 5:1, 2:1) demonstrate broad d−d transition bands ($\lambda_{max} \approx 850$ ($\epsilon_M \approx 8$), 1180 ($\epsilon_M \approx 8$) nm) which are most closely related to those exhibited in n-IR/ATR spectra of solid **4** (Figure 2, bottom insets). We also note that the electronic spectrum of **2** (10^{-5}–10^{-3} M) in pyridine or py/AcOH (10:1, 5:1, 2:1) is identical with that exhibited by **3/4** and accounts for greater than 90% conversion of **2** to **3/4** (Figure 2, top inset). These results suggest that addition of Et$_2$O or employment of nonpyridine solvents is essential for the generation of **2**.

The precise nature of species **4** in pyridine or py/AcOH solutions is not easily discernible. It is unlikely that infinite chains of **4** will be present in solution, although the degree of aggregation can be substantial in the polar py/AcOH matrix.[55] However, electrospray MS data obtained at various initial concentrations of **3** in py/AcOH (10:1) have only yielded fragments assigned to [Fe(OAc)(py)]$^+$, [Fe(OAc)(py)$_2$]$^+$, [Fe$_2$(OAc)$_3$(py)]$^+$, [Fe$_2$(OAc)$_3$(py)$_2$]$^+$, [Fe$_3$(OAc)$_5$(py)]$^+$, and [Fe$_3$(OAc)$_5$(py)$_2$]$^+$. The trinuclear fragments become apparent at higher initial concentrations ([**3**] $\geq 0.88 \times 10^{-3}$ M), although the effective concentration of **3** in the droplet (travelling against a countercurrent of inert gas) from which the ions desorb is not

known. ^{1}H NMR spectra of **3** in pyridine or py/ACOH are not very informative, even at low temperatures, owing to the rapid exchange of pyridine/acetate moieties among the various iron-containing species and the solvent matrix. In CD$_2$Cl$_2$ (as well as in other non-pyridine solvents), chemical shifts for pyridine/acetate groups of **3/4** are concentration-dependent, the degree of isotropic shift diminishing with decreasing concentration. It is noteworthy that **3** is crystallized from saturated solutions of **3** in CH$_2$Cl$_2$, while diffusion of Et$_2$O into CH$_2$Cl$_2$ affords a microcrystalline product that is analytically identical to compound **4**. Antiferromagnetically coupled dinuclear and higher nuclearity species are expected to demonstrate isotropically shifted NMR spectra of reduced range by comparison to their mononuclear counterparts.

The slow reaction of Zn with AcOH results in the formation of solubilized zinc acetate products which participate in equilibria in parallel to, as well as along with iron species. Compound **5** is consistently obtained along with other iron-containing species from pyridine or py/AcOH (10:1, 5:1) Gif-type solutions. It can also be crystallized pure from similar solutions of Zn(O$_2$CCH$_3$)$_2$·2H$_2$O, albeit in two distinct crystal systems: tetragonal in pyridine or py/AcOH (10:1) and triclinic from py/AcOH (5:1). The aforementioned dissociation of **2** in pyridine or py/AcOH (10:1) to generate **3** and **5** also affords crystals of **5** in the tetragonal crystal system. However, solutions of **5** in py/AcOH (2:1) yield exclusively [Zn$_2$(O$_2$CCH$_3$)$_4$(py)$_2$] (**6**) upon crystallization. Compound **6** usually crystallizes in the monoclinic system, although on a single occasion it has also been crystallized from py/AcOH (2:1) in the orthorhombic crystal system, as one of the products of the oxidation of **2** (vide infra). Variable-concentration and -temperature ^{1}H NMR spectra of **5** in pyridine or py/AcOH are not sufficiently diagnostic, most likely due to rapid ligand exchange even at low temperatures. However, CI-MS data reveal that the molecular ion of **5** ($m/z = 341.7$) and fragments of **6** are solely detected from py/AcOH solutions, the latter being more pronounced for samples in py/AcOH (2:1). It thus appears that, in Gif-type solutions, zinc is present in the form of **5** and **6**. Higher nuclearity species have been detected and isolated only from non-pyridine solvents. The one-dimensional chain compound [Zn(O$_2$CCH$_3$)$_2$(py)]$_n$ (**7**) is obtained from solutions of **5** in EtOH or CH$_2$Cl$_2$, while the trinuclear [Zn$_3$(O$_2$CCH$_3$)$_6$(py)$_2$] (**8**) is deposited from solutions of **5** in CH$_3$CN or **6** in CH$_2$Cl$_2$. As in the case of **4**, the nature of **7** in solution is not precisely known, but interestingly, this species is isomeric to **6**.

Other Reducing Agents. Although Zn dust is the most practical source of reducing equivalents, compounds **3** and **4** can also be isolated by treatment of **1** with excess iron dust in pyridine or py/AcOH (10:1) for 30 min and from the reaction of **1** with H$_2$(30 psig)/Pd in pyridine or py/AcOH (10:1) for 1 h. Both reactions, after removal of insoluble components, afford bright yellow-green solutions from which high yields of compounds **3/4** are crystallized as previously described. A control experiment confirmed that these species are also generated by simply stirring Fe in py/AcOH (10:1). Iron has been previously used as a reducing agent in the early Gif^{III} (Fe/O$_2$, 40 °C) catalytic version,[56] yielding results nearly identical to those of Gif^{IV} systems. Apparently, the two systems are equivalent with respect to their solvated iron-containing species.

Related Ferrous Species. We have also explored the possibility of anionic ferrous species being formed in Gif-type solutions owing to the nature of the solvent matrix (py/AcOH) involved. The potential role of water in modifying the structural elements of the observed ferrous sites has also drawn our

(55) Golubev, N. S.; Smirnov, S. N.; Gindin, V. A.; Denisov, G. S.; Benedict, H.; Limbach, H.-H. *J. Am. Chem. Soc.* **1994**, *116*, 12055−12056.

(56) (a) Barton, D. H. R.; Gastiger, M. J.; Motherwell, W. B. *J. Chem. Soc., Chem. Commun.* **1983**, 41−43. (b) Barton, D. H. R.; Motherwell, R. S. H.; Motherwell, W. B. *Tetrahedron Lett.* **1983**, 1979−1982.

attention, since addition of water to py/AcOH (10:1) up to an optimum amount of 6.6% w/w is known[36a] to enhance the selectivity of Gif chemistry.

Addition of [Ph$_3$P=N=PPh$_3$][O$_2$CCH$_3$] (1 equiv) to **3** in pyridine affords yellow needles of [PPN][Fe^{II}(O$_2$CCH$_3$)$_3$(py)] (**9**) upon diffusion of Et$_2$O at room temperature. In contrast, a mixture of predominantly **3** and a minor amount of **9** are deposited directly from concentrated pyridine solution at −20 °C. Solutions of **3** in py/H$_2$O (10:1) or py/AcOH/H$_2$O (10:1: 0.7) afford yellow crystals of [Fe^{II}(H$_2$O)$_4$(*trans*-py)$_2$][O$_2$CCH$_3$]$_2$ (**10**) upon slow diffusion of Et$_2$O. Compound **10** reverses quantitatively to **3** in neat pyridine as evidenced by isolation of **3** (−20 °C). UV−vis spectra of **10** in pyridine or py/H$_2$O exhibit features identical to those observed for **3** ([**10**] < 1.0 × 10^{-3} M), indicating complete dissociation of the water adduct in favor of the pyridine-ligated species.

The lability of pyridine is also demonstrated thermogravimetrically in its facile thermal (50 °C) dissociation from **3** under vacuum (0.01 Torr), leading to the successive loss of two (1.5 h), three (2.5 h), and finally four (6 h) pyridine equivalents to yield Fe(OAc)$_2$. The purity and identity of the intermediate products cannot be easily elucidated, since employment of nonpyridine solvents to dissolve these species further contributes to pyridine dissociation. This is dramatically shown in the case of the prolonged incubation (2 d) of **3** in DMSO-d_6 that leads to precipitation of colorless, air-sensitive crystals of [Fe^{II}$_3$(O$_2$CCH$_3$)$_6$(OS(CD$_3$)$_2$)$_2$]$_n$ (**11**). Compound **11** is also obtained from solutions of Fe(O$_2$CCH$_3$)$_2$ in DMSO.

Reaction of Ferrous Species with Dioxygen. Upon exposure of concentrated pyridine or py/AcOH (10:1) solutions of **3** and **4** to pure dioxygen or air, compound **1** can be isolated in essentially quantitative yields. However, preliminary UV−vis studies have indicated that oxidation of solutions of **3** with dry oxygen at concentrations below 0.88 × 10^{-3} M (in py/AcOH (10:1)) and 1.0 × 10^{-3} M (in neat pyridine) generates an intermediate (λ_{max} = 338 (py/AcOH), 344 (py) nm) that only partially and slowly converts to **1**. This intermediate can be observed even after 24 h. A broad but rather weak absorption centered at 658 nm is also detected in dilute py/AcOH (10:1) solutions (for instance, [**3**] = 0.65 × 10^{-4} M). In addition to absorbances assigned to **1** (λ = 358, 416, 488, 580 nm in py/AcOH (10:1)), a feature at 474 nm grows in, associated with a decay product. Interestingly, similar absorbances at 474 and 670 (broad transient) nm have been recently detected[57] in the oxidation of [Fe$_2$(OH)(Me$_3$TACN)$_2$(OAc)$_2$]$^+$ and attributed to diiron μ-oxo and μ-peroxo species, respectively. Efforts to isolate and characterize the observed intermediates are currently underway. In contrast, at concentrations of **3** above the threshold values, the onset of a much more rapid and complete generation of **1** is progressively observed under similar conditions with no well-resolved intermediates being detected by conventional UV−vis techniques. For instance, oxidation of solutions of **3** (1.3 × 10^{-3} M) in py/AcOH (10:1) generates essentially quantitative amounts of **1** within 1 h. At these higher concentrations, the anticipated generation of **4** in py/AcOH solutions may drastically influence the rate and/or nature of dioxygen activation. A detailed kinetic analysis of the formation and decay of intermediates is currently in progress by means of cryostopped-flow mixing of reactants and rapid diode array detection.[58]

The reaction of **2** with dioxygen in py/AcOH (10:1) affords red-black crystals of [Fe$_{2.22(2)}$Zn$_{0.78(2)}$O(O$_2$CCH$_3$)$_6$(py)$_3$]·py (**1′**). The supernatant (py/AcOH (2:1) after solvent reduction) yields

colorless orthorhombic crystals of [Zn$_2$(O$_2$CCH$_3$)$_4$(py)$_2$] (**6**). Compound **1′** is readily distinguished from **1** by virtue of its isotropically shifted ^{1}H NMR, ^{57}Fe Mössbauer effect (10% of Fe(II)), and precise Fe/Zn composition derived from ICP microanalysis. Scanning electron microprobe analysis performed on 10 single crystals of **1′** confirms that each individual crystal contains zinc (Fe:Zn = 74:26). These results along with X-ray diffraction analysis and literature precedence[59] establish that compound **1′** is neither a collection of crystals of **1** and **1″** nor an agglomeration of distinct phases of **1** and **1″** in a single crystal of **1**. As suggested by the method of preparation of **1″**,[51] a minimum of a 5-fold excess of solvated Zn(II) over Fe(II) is necessary for complete occupancy of the divalent site of the μ-oxo structure by zinc after oxidation.

Admittance of dioxygen to the filtrate of the prolonged reduction (6 h) of **1** by Zn in pyridine deposits dichroic red−green crystals of monoclinic **1″**. Interestingly, compound **1″**, prepared by the original method,[51] crystallizes in the rhombohedral crystal system. The isolation of **1″** indicates that, in catalytic oxidations in which excess Zn is in contact with py/AcOH (10:1) for 18 h, compound **1″** may be more involved as the product of autoxidation than the all-iron species **1**.

Solid State Structures. (a) Iron Species in Gif Solutions. Among the various stoichiometries reported, only species **1/1′/1″** and **3/4** can be legitimately claimed to be present in pyridine or py/AcOH solutions, with the aforementioned reservations in regards to the precise nature of **4** in these solutions taken into account. Compound **1′** (Figure 3, top) crystallizes in space group *R*32, featuring trinuclear metal μ-oxo clusters with crystallographically imposed D_3 symmetry. The occupancy of each metal site was fixed at Fe 0.37 and Zn 0.13, based on analytical data. Disorder of the trinuclear unit at 223 K does not allow the different metal sites to be distinguished. Each M−O(1) vector (1.914(1) Å) lies along a C_2 axis, while O(1) resides on a perpendicular C_3 axis. As previously revealed in similar structures,[45] the solvated pyridine is sandwiched along the C_3 axis between two stacked trinuclear clusters and is severely disordered. In contrast, the structure of compound **1″** (Figure 3, bottom), synthesized by the in situ oxidation of reduced (6 h) solutions of **1** by Zn in pyridine (vide supra), displays the more rarely observed monoclinic crystal system that, lacking a C_3 axis, distinguishes between two metal sites by virtue of a crystallographically imposed C_2 axis. This axis penetrates atoms O(1), M(2), N(2), and C(14). M(1) and M(2) represent metal sites of occupancy Zn(1/3)/Fe(2/3) and Zn(1/6)/Fe(1/3), respectively. The M(1)−O(1) vectors (1.929(3) Å) are slightly longer than the unique M(2)−O(1) vector (1.900-(6) Å) but not sufficiently different to allow exclusive assignment of M(1) and M(2) sites to Fe(III) and Zn(II), respectively.

The structure of mononuclear **3** (Figure 4) reveals a distorted octahedral Fe environment with an imposed C_2 axis residing in the equatorial plane defined by the four Fe−N bonds and bisecting the symmetry-related N(1)−Fe−N(1A) (89.1(2)°) and N(2)−Fe-N(2A) (92.2(2)°) angles. Pyridine rings are arranged in a propeller fashion around the equatorial plane. Relevant to the observed distortion are the Fe−N(1) and Fe−N(2) bond distances as well as the O(1)−Fe−N(1) and O(1)−Fe−N(2) bond angles which slightly differ from each other. The most visible sign of the distortion is the departure from linearity of the angle between the two trans acetate groups along the propeller axis (O(1)−Fe−O(1A) = 168.5(2)°).

The structure of **4** (Figure 5) reveals a one-dimensional polymer chain comprised of asymmetric diferrous units. In the unit cell, the chains run parallel to the 2$_1$ screw axis (along the

(57) Feig, A. L.; Masschelein, A.; Bakac, A.; Lippard, S. J. *J. Am. Chem. Soc.* **1997**, *119*, 334−342.

(58) Kaderli, S.; Singh, B.; Stavropoulos, P.; Zuberbühler, A. D. Work in progress.

(59) Jang, H. G.; Kaji, K.; Sorai, M.; Wittebort, R. J.; Geib, S. J.; Rheingold, A. L.; Hendrickson, D. N. *Inorg. Chem.* **1990**, *29*, 3547−3556.
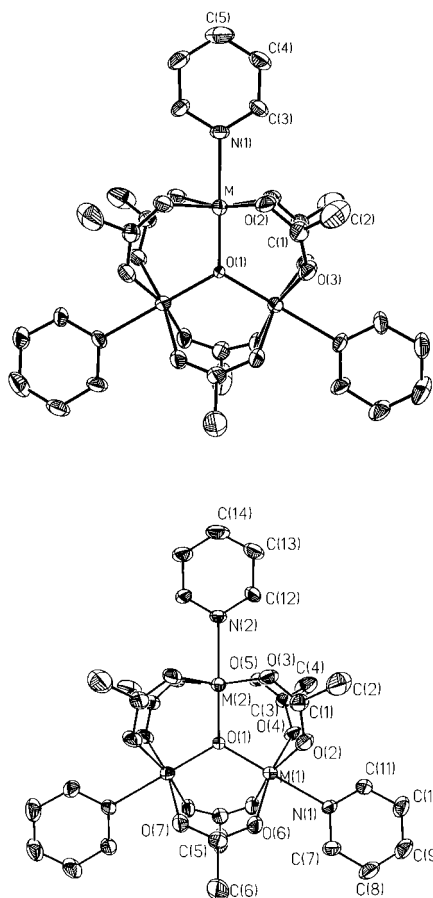
Figure 3. Structures of trigonal [Fe$_{2.22(2)}$Zn$_{0.78(2)}$O(O$_2$CCH$_3$)$_6$(py)$_3$]·py (**1′**) (top) and monoclinic [Fe$_2$ZnO(O$_2$CCH$_3$)$_6$(py)$_3$]·py (**1″**) (bottom) showing 40% and 30% probability ellipsoids, respectively and the atom labeling schemes. Selected interatomic distances (Å) and angles (deg) for **1′**: M−O(1) 1.914(1), M−O(2) 2.042(5), M−N(1) 2.203(7), O(1)−M−O(2) 96.2(2), O(1)−M−N(1) 180.0(1), O(2)−M−N(1) 83.8(2); **1″**: M(1)−O(1) 1.929(3), M(1)−O(2) 2.057(6), M(1)−O(4) 2.075(6), M(1)−N(1) 2.202(9), M(2)−O(1) 1.900(6), M(2)−O(3) 2.072(7), M(2)−O(5) 2.041(6), M(2)−N(2) 2.211(8), O(1)−M(1)−O(2) 96.2-(3), O(1)−M(1)−O(4) 95.3(3), O(2)−M(1)−O(4) 89.1(3), O(1)−M(1)−N(1) 179.7(2), O(1)−M(2)−O(3) 95.3(2), O(1)−M(2)−O(5) 96.2(2), O(3)−M(2)−O(5) 89.8(3), O(1)−M(2)−N(2) 180.0(1), M(1)−O(1)−M(2) 120.2(2).
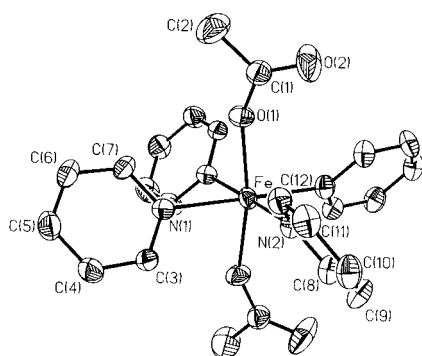
Figure 4. Structure of the mononuclear [Fe^{II}(O$_2$CCH$_3$)$_2$(py)$_4$] (**3**) compound showing 50% probability ellipsoids and the atom labeling scheme. Selected interatomic distances (Å) and angles (deg): Fe−O(1) 2.031(4), Fe−N(1) 2.240(5), Fe−N(2) 2.213(5), O(1)−Fe−N(1) 85.8-(2), O(1)−Fe−N(2) 94.1(2), N(1)−Fe−N(2) 89.4(2), O(1)−Fe−O(1A) 168.5(2).

c axis). Each dinuclear unit is bridged to two adjacent units via O(8) and O(7A) (Fe(1)···Fe(2′) = 5.275 Å). The essentially octahedral Fe(1) atom is coordinated by two N(py) donor atoms and four acetate-derived oxygen atoms, featuring a slight elongation along the O(1)−Fe(1)−N(2) direction. The much
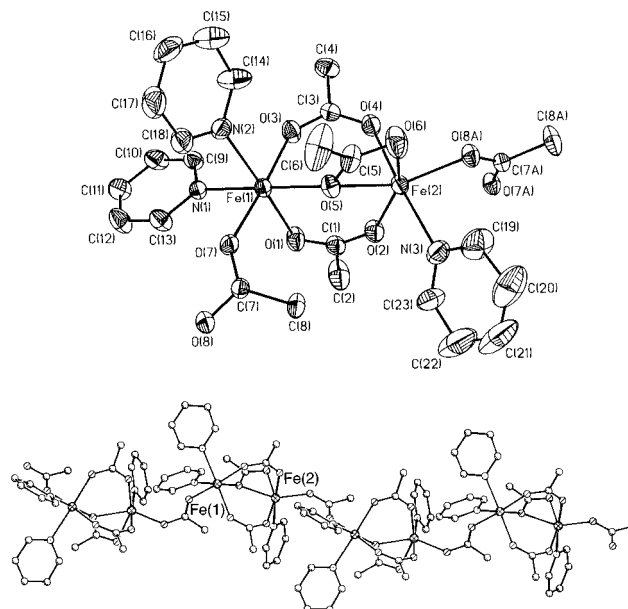
Figure 5. Structure of the local dinuclear geometry (top) and one-dimensional chain (bottom) of [Fe$^{II}_2$(O$_2$CCH$_3$)$_4$(py)$_3$]$_n$ (**4**) showing 30% probability ellipsoids and the atom labeling scheme. Selected interatomic distances (Å) and angles (deg): Fe(1)−O(7) 2.073(4), Fe(1)−O(3) 2.076(4), Fe(1)−O(1) 2.157(4), Fe(1)−O(5) 2.179(4), Fe(1)−N(1) 2.228(4), Fe(1)−N(2) 2.247(4), Fe(2)−O(2) 2.033(4), Fe(2)−O(4) 2.117(4), Fe(2)−O(5) 2.212(3), Fe(2)−N(3) 2.259(5), Fe(2)−O(6) 2.273(5), O(7)−Fe(1)−O(1) 92.9(2), O(3)−Fe(1)−O(1) 90.6(2), O(1)−Fe(1)−O(5) 92.6(2), O(5)−Fe(1)−N(1) 178.61(14), O(1)−Fe(1)−N(2) 175.4(2), O(2)−Fe(2)−O(5) 96.00(14), O(8A)−Fe(2)−O(5) 142.76-(14), O(2)−Fe(2)−O(6) 152.9(2), O(4)−Fe(2)−O(6) 93.7(2), O(5)−Fe(2)−O(6) 57.4(2), N(3)−Fe(2)−O(6) 88.7(2).

more distorted Fe(2) site is surrounded by an O$_5$/N ligating environment. The two iron atoms of the asymmetric core (Fe-(1)···Fe(2) = 3.676 Å) are bridged by two bidentate acetate groups and a unique monodentate acetate bridge which also serves as a bidentate chelator to Fe(2). The metric parameters associated with the shift from a bridging monodentate to an ancillary chelating position (termed "the carboxylate shift") have been discussed in the literature,[60] the degree of the "shift" varying with the extent of contact of the distal oxygen atom with the iron site. The one observed in **4** (Fe(2)−O(6) = 2.273-(5) Å) is a rare case of a strong bonding interaction (comparable to Fe(2)−O(5) = 2.212(3) Å), instances of which are only found in the structures of Fe$_3$(O$_2$CPh)$_6$L$_2$ (L = ^{i}PrOx, PheMe$_3$Eda),[61] the dimetallic Mn(II)Ca(II) site of concanavalin A,[62] and, more relevantly, the diiron site of the H$_{red}$ component of sMMO (Fe−O(Glu243) = 2.33 Å).[6a,b] Indeed, the corresponding Fe(2) sites of **4** and H$_{red}$ in sMMO demonstrate remarkable metrical similarities with respect to the arrangement of their respective O$_5$/N coordination sphere, although the sMMO site is closer to being five-coordinate. The most pronounced difference is the existence of a weakly bound semibridging water molecule in H$_{red}$ in lieu of a bridging bidentate acetate in **4**. The monodentate water bridge may be responsible for the relative shrinkage of the reported Fe···Fe distance (3.28 Å) in H$_{red}$ versus the corresponding distance in **4**. The coordination sphere of

(60) Rardin, R. L.; Tolman, W. B.; Lippard, S. J. *New J. Chem.* **1991**, *15*, 417−430.

(61) (a) Goldberg, D. P.; Telser, J.; Bastos, C. M.; Lippard, S. J. *Inorg. Chem.* **1995**, *34*, 3011−3024. (b) Rardin, R. L.; Poganiuch, P.; Bino, A.; Goldberg, D. P.; Tolman, W. B.; Liu, S.; Lippard, S. J. *J. Am. Chem. Soc.* **1992**, *114*, 5240−5249 and other references therein. (c) Tolman, W. B.; Liu, S.; Bentsen, J. G.; Lippard, S. J. *J. Am. Chem. Soc.* **1991**, *113*, 152−164.

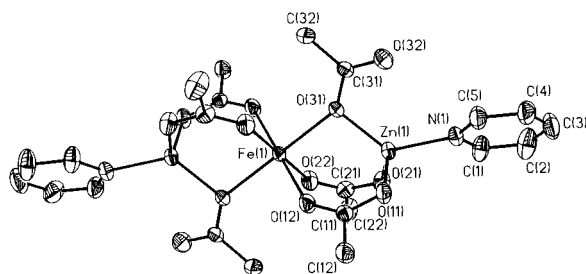(62) Hardman, K. D.; Agarwal, R. C.; Freiser, M. J. *J. Mol. Biol.* **1982**, *157*, 69−86.

Oxidation of Hydrocarbons under Gif-Type Conditions

J. Am. Chem. Soc., Vol. 119, No. 30, 1997 7041

Figure 6. Structure of the centrosymmetric compound [$Zn_2Fe^{II}(O_2$-$CCH_3)_6(py)_2$] (**2**) showing 40% probability ellipsoids and the atom labeling scheme. Selected interatomic distances (Å) and angles (deg): Fe(1)−O(12) 2.115(3), Fe(1)−O(22) 2.099(3), Fe(1)−O(31) 2.156(3), Zn(1)−O(11) 1.954(3), Zn(1)−O(21) 1.942(3), Zn(1)−O(31) 1.959-(3), Zn(1)−N(1) 2.017(4), O(12)−Fe(1)−O(22) 94.1(1), O(12)−Fe-(1)−O(31) 91.5(1), O(11)−Zn(1)−O(21) 112.0(1), O(11)−Zn(1)−O(31) 105.3(1), O(31)−Zn(1)−N(1) 129.2(1).

Fe(1) in **4** differs from the corresponding site in H_{red} both in being more nitrogen-rich and in the relevant orientation of the bridging versus the terminal residues.

(b) Other Ferrous Acetate Structures. The structure of **2** (Figure 6) reveals a linear arrangement of three metal sites, featuring an essentially octahedral centrosymmetric iron atom bridged to two tetrahedrally ligated zinc atoms. The bridging moieties are provided by two bidentate and one monodentate acetate groups. A slight elongation along the O(31)−Fe(1)−O(31′) axis (Fe(1)−O(31) = 2.156(3) Å) of the exclusively oxygen-coordinated iron site is observed. The tetrahedral geometry of the outer zinc atoms is distorted, especially with respect to the position of the bridging oxygen atom of the monodentate acetate group versus the nitrogen atom of pyridine (O(31)−Zn(1)−N(1) = 129.2(1)°). A similar arrangement of bridging acetate groups has been observed in homonuclear and heteronuclear $M_2M'(O_2CCR_3)_6L_2$ structures (M = V, Mn, Fe, Co, Zn; M' = V, Mn, Fe, Co, Ni, Zn, Cd, Mg, Ca, Sr; L = substituted pyridines or bidentate N-donor ligands)[61b] although the Zn_2Fe combination was unknown. Of particular interest in this series of compounds are the aforementioned trinuclear iron species of stoichiometries $Fe_3(O_2CR)_6L_2$ (R = Me, L = BIPhMe, BIPhOH, BIDPhEH; R = Ph, L = ^iPrOx, PheMe$_3$-Eda)[61a] in which the outer iron atoms are additionally coordinated (weakly or strongly) by the distal oxygen atom of the monodentately bridging acetate.

The structure of compound **9** (Figure 7) reveals a pseudo-seven-coordinate iron center coordinated by three asymmetrically chelating acetate groups and a unique pyridine moiety. The asymmetry of the bidentate chelation is evident from the Fe−O(1) (2.087(3) Å) and Fe−O(2) (2.313(3) Å) distances and becomes more pronounced with the other two acetates, since both O(4) and O(6) assume positions of interatomic contact with the iron center (Fe···O(4/6) = 2.829 Å).

The structure of compound **10** (Figure 8) reveals an octahedral iron site residing on an inversion center and coordinated by four water molecules in the equatorial plane and two pyridine molecules along a perpendicular axis. All hydrogen atoms, with the exception of those on the Me group of the acetate, were located in the electron density map and refined isotropically. Each hydrogen atom belonging to a coordinating water molecule makes a hydrogen bond with an acetate oxygen atom. The two noncoordinating acetates associated with the cationic iron center form hydrogen bonds with *cis*-water molecules in a bidentate fashion (O(3)−H(1A) = 1.92 Å, O(4)−H(2A) = 1.91 Å; O(3)···O(1) = 2.680 Å, O(4)···O(2) = 2.680 Å). In addition, each acetate is hydrogen-bonded to two adjacent cationic units (O(3)−H(1B) = 1.98 Å, O(4)−H(2B) = 2.00 Å), leading to an overall two-dimensional sheet network structure.
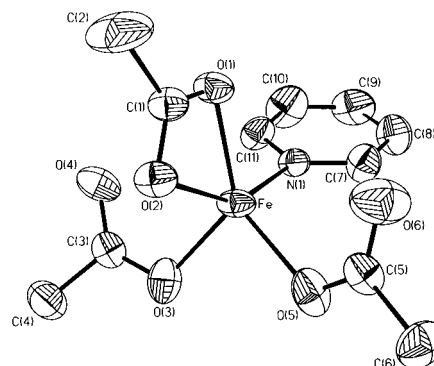

Figure 7. Structure of the anionic component of [PPN][$Fe^{II}(O_2CCH_3)_3$-(py)] (**9**) showing 30% probability ellipsoids and the atom labeling scheme. Selected interatomic distances (Å) and angles (deg): Fe−O(5) 2.033(4), Fe−O(3) 2.059(4), Fe−O(1) 2.087(3), Fe−O(2) 2.313(3), Fe−N(1) 2.160(4), O(5)−Fe−O(3) 90.1(2), O(5)−Fe−O(1) 135.3(2), O(3)−Fe−O(1) 129.5(2), O(5)−Fe−N(1) 99.3(2), O(3)−Fe−N(1) 104.0(2), O(1)−Fe−N(1) 90.8(2), O(5)−Fe−O(2) 104.04(14), O(3)−Fe−O(2) 94.96(14), O(1)−Fe−O(2) 59.05(13), N(1)−Fe−O(2) 149.72-(14).
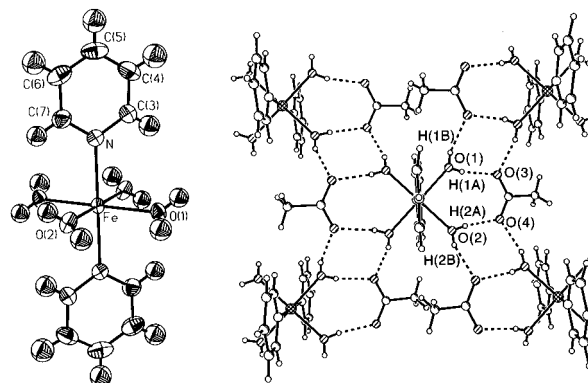

Figure 8. Structure of the local environment of the cation (left) and 2-D sheet network (right) of centrosymmetric [$Fe^{II}(H_2O)_4$(*trans*-py)$_2$][O_2CCH_3]$_2$ (**10**) showing 40% probability ellipsoids and the atom labeling scheme. Selected interatomic distances (Å) and angles (deg): Fe−O(1) 2.122(2), Fe−O(2) 2.122(2), Fe−N 2.213(2), O(1)−Fe−O(2) 90.32(10), O(1)−Fe−N 92.83(10), O(2)−Fe−N 92.67(10).

The crystal structure of **11** (Figure 9) was obtained from a crystal grown in solutions of DMSO-d_6. The compound is a one-dimensional solid containing chains comprised of two types of iron in a 2:1 (Fe(1):Fe(2)) ratio. Two Fe(1) centers are intimately coupled by one bidentate and two monodentate acetate bridges (Figure 9, top), although each of the distal oxygens of the monodentate acetate groups coordinates to an adjacent Fe(2) site. A crystallographically imposed C_2 axis penetrates atoms C(7) and C(8) of the bidentate acetate group. In addition, each Fe(1) is coordinated by one DMSO and two acetate groups. The latter are both bridging to the adjacent unique Fe(2) site (Figure 9, middle). One of them is a typical bidentate acetate, while the other is a unique monodentate bridge which also acts as a chelator to Fe(2). By virtue of a C_2 axis passing through atoms Fe(2), C(5), and C(6), the latter oxygen atom is also bridging the iron sites of the adjacent Fe(1)$_2$ unit; thus, this acetate spans the range Fe(1)$_2$···Fe(2)···Fe(1)$_2$ (Figure 9, bottom).

(c) Structures of Zn-Containing Species. Two crystallographic versions of **5** have been obtained. Presumably, they represent closely spaced energetic minima. The compound obtained in the tetragonal space group $P4_32_12$ (Figure 10, top), reveals a tetrahedral zinc site residing on a crystallographically imposed C_2 axis bisecting the N−Zn−N(A) (110.7(3)°) and O(1)−Zn-(O1A) (98.0(3)°) angles. Distortions from tetrahedral
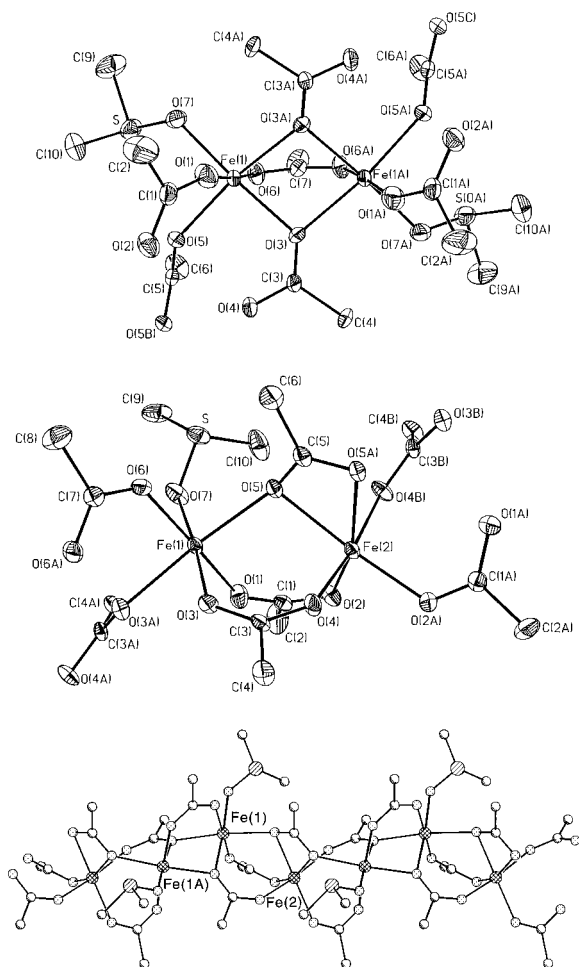
Figure 9. (top) Structure of the local environment of the equivalent Fe(1) sites (appoximately down the C_2 axis) in the one-dimensional $[Fe^{II}_3(O_2CCH_3)_6(OS(CD_3)_2)_2]_n$ (**11**) showing 40% probability ellipsoids and the atom labeling scheme. (middle) Structure of the bridging arrangement to the unique Fe(2) site showing 30% probability ellipsoids and the atom labeling scheme. A C_2 axis passes through atoms C(6), C(5), and Fe(2). (bottom) Overview of the one-dimensional chain structure of **11**. Selected interatomic distances (Å) and angles (deg): Fe(1)−O(1) 2.042(4), Fe(1)−O(6) 2.057 (4), Fe(1)−O(7) 2.130(4), Fe-(1)−O(3) 2.134(4), Fe(1)−O(5) 2.223(3), Fe(2)−O(2) 2.060(4), Fe-(2)−O(4) 2.119(4), Fe(2)−O(5) 2.236(4), O(1)−Fe(1)−O(3) 95.8(2), O(1)−Fe(1)−O(5) 93.5(2), O(3A)−Fe(1)−O(5) 171.97(13), O(3)−Fe-(1)−O(5) 93.68(13), O(5)−Fe(1)−O(7) 89.38(14), O(5)−Fe(2)−O(5A) 58.8(2), O(2)−Fe(2)−O(5) 104.5(2), O(4)−Fe(2)−O(5) 85.3(2), O(2)−Fe(2)−O(4) 103.1(2), O(2A)−Fe(2)−O(5A) 104.5(2).

symmetry are made evident by the latter angle and are likely due to two long-range Zn···O(2) interactions. Compound **5** crystallized in the triclinic space group $P\bar{1}$ with a slightly different geometry (Figure 10, bottom). The two structures differ primarily in the relative positions of the two long-range Zn···O contacts.

Crystals of compound **6** are also obtained in two crystal-lographic versions. In its monoclinic form, the dinuclear molecule (Figure 11) resides on a C_2 axis which penetrates atoms C(7), N(1), Zn(1), Zn(2), N(2), and C(10). In its orthorhombic form (see Supporting Information), the compound lies on an inversion center midway along the internuclear axis. The only noteworthy difference between the two structures lies in the torsion angles made by the planes of the two axial pyridine ligands.

The structure of compound **7** (Figure 12) reveals an extended one-dimensional solid comprised of an array of five-coordinate zinc centers. The chain repeat unit is defined by two zinc centers, Zn(1) and Zn(2). Each zinc atom is bridged to two
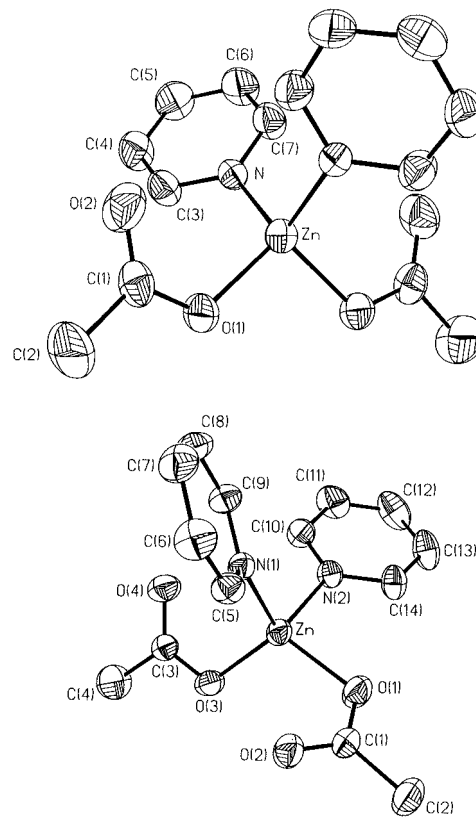
Figure 10. Structures of tetragonal (top) and triclinic (bottom) [Zn-(O_2CCH_3)_2(py)_2] (**5**) showing 30% probability ellipsoids and the atom labeling scheme. Selected interatomic distances (Å) and angles (deg) for tetragonal **5**: Zn−O(1) 1.941(4), Zn−N 2.021(5), O(1)−Zn−N 109.3(2); triclinic **5**: Zn−O(1) 1.945(2), Zn−O(3) 1.941(2), Zn−N(1) 2.047(2), Zn−N(2) 2.075(2), O(3)−Zn−O(1) 110.88(9), O(3)−Zn−N(1) 113.47(8), O(1)−Zn−N(1) 115.16(10), O(3)−Zn−N(2) 112.46-(9), O(1)−Zn−N(2) 96.45(8), N(1)−Zn−N(2) 107.16(8).
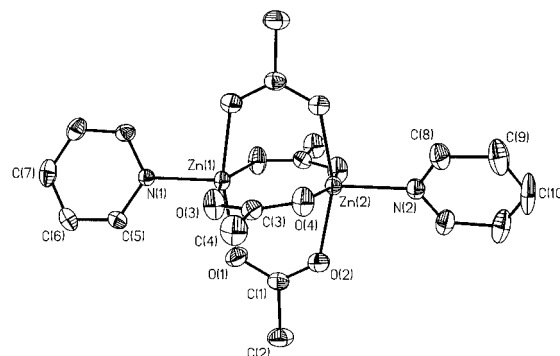

Figure 11. Structures of monoclinic [Zn_2(O_2CCH_3)_4(py)_2] (**6**) showing 30% probability ellipsoids and the atom labeling scheme. The structure of orthorhombic **6** is similar. Selected interatomic distances (Å) and angles (deg) for monoclinic **6**: Zn(1)−N(1) 2.037(5), Zn(1)−O(3) 2.041(3), Zn(1)−O(1) 2.042(3), Zn(1)···Zn(2) 2.8921(10), Zn(2)−O(2) 2.027930, Zn(2)−O(4) 2.042(3), Zn(2)−N(2) 2.047(5), N(1)−Zn(1)−O(3) 101.07(10), N(1)−Zn(1)−O(1) 98.87(10), O(3)−Zn(1)−O(1) 87.4(2).

neighbors by a bidentate acetate and is further coordinated by a pyridine and an asymmetrically chelating acetate group. Pyridine rings are oriented nearly perpendicular to each other at adjacent Zn sites. Most importantly, the chelating acetate groups are nonequivalent and asymmetric at these Zn centers (Zn(1)−O(1) = 2.024(6) Å, Zn(1)−O(2) 2.414(7) Å; Zn(2)−O(3) = 2.116(6) Å, Zn(2)−O(4) 2.255(7) Å).

Compound **8** (Figure 13) is isostructural with **2**, featuring a trinuclear zinc molecule residing on an inversion center. The unique octahedral zinc atom is bridged via two bidentate and
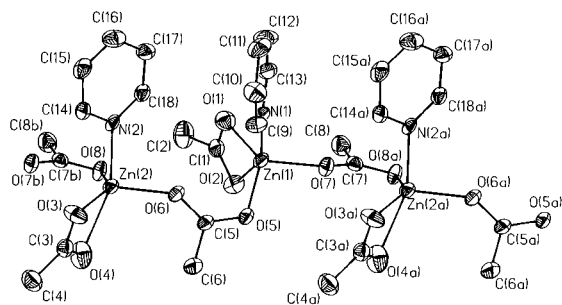
Figure 12. Structure of the one-dimensional $[Zn(O_2CCH_3)_2(py)]_n$ (**7**) chain showing 30% probability ellipsoids and the atom labeling scheme. Selected interatomic distances (Å) and angles (deg): Zn(1)−O(1) 2.024-(6), Zn(1)−O(2) 2.414(7), Zn(1)−O(5) 1.974(5), Zn(1)−O(7) 1.979-(5), Zn(1)−N(1) 2.065(6), Zn(2)−O(3) 2.116(6), Zn(2)−O(4) 2.255(7), Zn(2)−O(6) 1.987(5), Zn(2)−O(8) 1.999(5), Zn(2)−N(2) 2.068(6), O(1)−Zn(1)−O(2) 57.2(2), O(1)−Zn(1)−O(5) 131.7(2), O(2)−Zn(1)−O(5) 94.1(2), O(5)−Zn(1)−N(1) 103.3(2), O(3)−Zn(2)−O(4) 57.7-(2), O(3)−Zn(2)−O(6) 119.7(2), O(3)−Zn(2)−O(8) 138.6(2), O(3)−Zn(2)−N(2) 94.4(2).
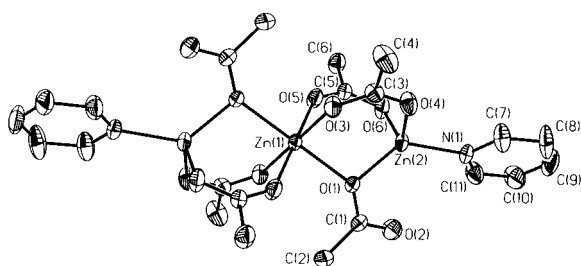
Figure 13. Structure of the centrosymmetric $[Zn_3(O_2CCH_3)_6(py)_2]$ (**8**) compound showing 30% probability ellipsoids and the atom labeling scheme. Selected interatomic distances (Å) and angles (deg): Zn(1)−O(1) 2.130(3), Zn(1)−O(3) 2.049(3), Zn(1)−O(5) 2.102(3), Zn(2)−O(1) 1.95193, Zn(2)−O(4) 1.946(3), Zn(2)−O(6) 1.951(3), Zn(2)−N(1) 2.016(3), O(1)−Zn(1)−O(3) 89.2(1), O(3)−Zn(1)−O(5) 93.2(1), O(4)−Zn(2)−O(6) 111.2(1), O(1)−Zn(2)−N(1) 130.7(1), Zn(1)−O(1)−Zn(2) 104.7(1).

one monodentate acetate groups to the outer tetrahedral zinc sites. Metric parameters are virtually identical with those observed in **2**. Structures similar to **6** and **8** have been reported for compounds of stoichiometry $Zn_2(carboxylate)_4(base)_2$ and $Zn_3(carboxylate)_6(base)_2$, respectively.[63]

Mössbauer Spectroscopy and Magnetization Studies. All iron-containing compounds presented in this investigation have been studied by ^{57}Fe Mössbauer spectroscopy. The zero-field spectra of the ferrous pyridine/acetate compounds (**2**−**4** and **9**−**11**) exhibit quadrupole doublets at isomer shifts and quadrupole splitting parameters characteristic of high-spin ferrous sites ($S = 2$). The isomer shift values for the neutral species **2**−**4** and **11** indicate a trend that is consistent with increasing δ values as the amount of oxygen ligation increases versus nitrogen ligation. This trend has been previously suggested[4c] for Fe(III) species. Even in the case of the asymmetric diiron site of **4**, the zero-field Mössbauer spectrum in the solid state at 4.2 K (Figure 14, top) demonstrates a unique quadrupole doublet ($\delta = 1.27$ mm/s, $\Delta E_Q = 2.92$ mm/s, $\Gamma = 0.20$ mm/s), thus the two iron sites remain indistinguishable even at low temperature.[64] In contrast, the Mössbauer spectrum of **11** shows

(63) (a) Clegg, W.; Hunt, P. A.; Straughan, B. P.; Mendiola, M. A. *J. Chem. Soc., Dalton Trans.* **1989**, 1127−1131. (b) Clegg, W.; Little, I. R.; Straughan, B. P. *Inorg. Chem.* **1988**, 27, 1916−1923. (c) Clegg, W.; Little, I. R.; Straughan, B. P. *J. Chem. Soc., Dalton Trans.* **1986**, 1283−1288. (d) Clegg, W.; Little, I. R.; Straughan, B. P. *J. Chem. Soc., Chem. Commun.* **1985**, 73−74.

(64) For a similar case applying to the closely related species (Et_4N)[Fe_2(O_2-CCH_3)_5(H_2O)(py)_2], see: Coucouvanis, D.; Reynolds, R. A., III; Dunham, W. R. *J. Am. Chem. Soc.* **1995**, *117*, 7570−7571.
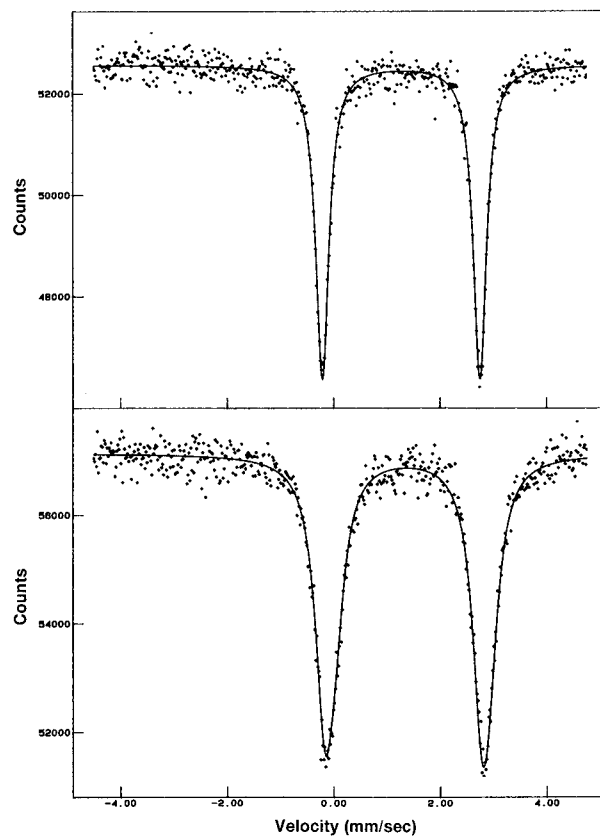

Figure 14. Mössbauer spectra at 4.2 K of polycrystalline **4** (top) and **11** (bottom). Solid lines are theoretical fits corresponding to a single ferrous site in the case of **4** and two superimposing ferrous sites in a ratio of 2:1 in the case of **11**.
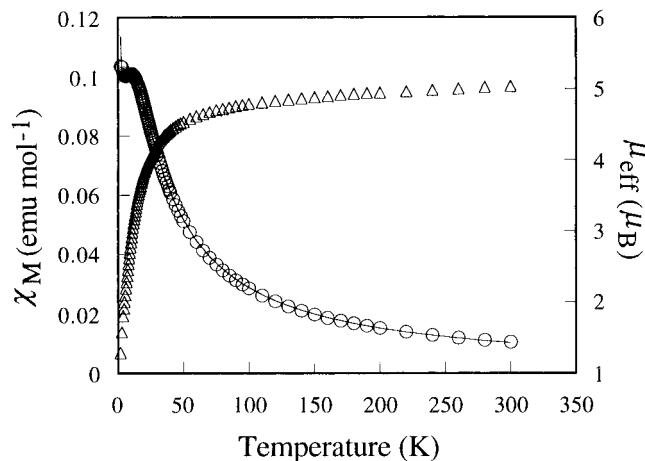

Figure 15. Plots of molar susceptibility (χ_M) per metal ion versus temperature (deg) and effective moment versus temperature (Δ) for compound **4**. The solid line is the best fit obtained as described in the text by employing the parameters deposited as Supporting Information.

a substantially broadened and rather asymmetric quadrupole doublet (Figure 14, bottom). The spectrum can be successfully fitted by virtue of two different ferrous sites at a ratio of 2:1 ($\delta = 1.40$ mm/s, $\Delta E_Q = 3.04$ mm/s, $\Gamma = 0.20$ mm/s, 66%; $\delta = 1.38$ mm/s, $\Delta E_Q = 2.94$ mm/s, $\Gamma = 0.22$ mm/s, 34%).

The measured magnetic susceptibility per iron ion of **4** as a function of temperature is shown in Figure 15. The μ_{eff} value of **4** at room temperature is 5.0 μ_B, close to the value expected for uncoupled Fe(II) ions. The molar susceptibility, χ_M, increases with decreasing temperature reaching a local maximum at 10 K ($\chi_M = 0.1012$ emu mol^{-1}). At lower temperatures, χ_M again increases, probably due to the presence of a paramagnetic impurity.

As mentioned earlier, the structure of **4** shows two largely different Fe⋯Fe distances (3.676 and 5.275 Å), and therefore, alternation of exchange coupling constants is anticipated. The shorter bridge, comprised of two bidentate and one monodentate as well as chelating acetate groups, is expected to be more efficient than the longer one in transmitting the magnetic interaction. The geometry between the closely spaced Fe ions is similar to that found in other metal ion dimers[61,65] and is known to mediate a small magnetic exchange between ferrous sites.[61] In contrast, the single bidentate acetato group, bridging the longer Fe⋯Fe separation, is expected to be very ineffective in transmitting exchange interactions. On this basis, magnetic data were first analyzed by using a simple dinuclear model, that is, setting the coupling constant along the longer bridge to zero. The magnetic susceptibility data were fitted to the analytical expression derived from the isotropic Heisenberg−Dirac−van Vleck model using the spin Hamiltonian 19 which consists of three terms describing the isotropic exchange, axial zero-field local anisotropy and Zeeman perturbation.

$$\hat{H} = -J S_1 \cdot S_2 + \sum_{i=1}^{2} D_i(S_{iz}^2 - S_i(S_i + 1)/3) + \mu_B G_i S_i H \quad (19)$$

The best fit of molar susceptibility data is shown in Figure 15 as a solid line and corresponds to $g = 2.077$, $J = -3.36$ cm^{-1}, and $D = -1.441$ cm^{-1}. The paramagnetic impurity was evaluated as 4.45 wt % of Fe(III) ($S = 5/2$), assuming oxidative decomposition of this exceedingly air-sensitive compound. The J value so obtained is in good agreement with values determined for similar, antiferromagnetically coupled compounds ($-20 \leq J \leq 0$ cm^{-1})[61,65] and in particular with small values ($J = -1.0$ cm^{-1}) reported for the similarly bridged species Fe$_3$(O$_2$CPh)$_6$L$_2$ (L = ^{i}PrOx, PheMe$_3$Eda).[61] The D value is also close to those reported for mononuclear zero-field splitting at individual sites of dinuclear ferrous systems.[66] Attempts were also made to analyze the data by means of a homogeneous chain model.[67] The spin Hamiltonian (eq 20) used to describe the magnetic interaction between adjacent ions in a regular magnetic chain and the analytical expression[68] (eq 21) employed to fit the data are as follows:

$$\hat{H} = -J \sum_{i=1}^{\infty} S_i S_{i+1} \quad (20)$$

$$\chi_r = \frac{T_r^2 + A T_r + B}{T_r^3 + C T_r^2 + D T_r + E} \quad (21)$$

where $\chi_r = 3\chi|J|/N\mu_B^2 g^2 S(S + 1)$ and $T_r = kT/|J|$ are the reduced susceptibility and temperature, respectively. The analytical expression is obtained by an extrapolation procedure on data calculated for closed chains (rings) of increasing size from 3 to

6 metal sites; a six-ion ring is the upper limit for $S = 2$ ions, due to the computational effort involved.

The fit with the six-metal model ($g = 2.059(3)$, $J = -2.011(7)$ cm^{-1}) was less satisfactory by comparison to the one obtained with the dinuclear model, confirming the suggestion that the two magnetic coupling constants, along the shorter and longer Fe⋯Fe distances, must be substantially different from each other. Unfortunately, analytical formulas for alternating chains of $S = 2$ ions are not currently available.

The μ_{eff} value of **11** at room temperature is 5.3 μ_B per ferrous ion, in agreement with independent spins. On decreasing temperature, μ_{eff} remains essentially constant down to ca. 10 K, rapidly decreasing beyond that point (see Supporting Information). The susceptibility χ_M continuously increases with decreasing temperature, but no maximum is observed, suggesting that the exchange coupling, if any, is close to zero.

Since the structure of **11** reveals similar Fe⋯Fe separation distances between neighboring ferrous sites (3.267, 3.543 Å), attempts were made to fit the magnetic data with the homogeneous chain model, even though the bridging geometry is different in the two cases. The parameters thus obtained are $g = 2.18(1)$ and $J = -0.22(1)$ cm^{-1}, but the fit (see Supporting Information) was quite poor for the data at lower temperatures. To our knowledge, no other models are available for a magnetic system of this complexity, the fitting being even more difficult due to the weakness of the magnetic interaction. No further attempts were undertaken to improve on the fitting procedure.

Catalytic Oxidations. Oxidation of adamantane mediated by **2**−**4** under Gif-type conditions affords the following products (unless otherwise specified, percentages are based on mol % of substrate conversion): 2-adamantanone (**2**, 10.7%; **3**, 10.7%; **4**, 10.1%), 2-adamantanol (**2**, 1.2%; **3**, 1.3%; **4**, 1.3%), 1-adamantanol (**2**, 0.8%; **3**, 0.9%; **4**, 0.7%), 4-(1-adamantyl)pyridine (**2**, 6.0%; **3**, 5.9%; **4**, 6.0%), and 2-(1-adamantyl)pyridine (**2**, 3.8%; **3**, 4.0%; **4**, 3.2%). Traces of 4-(2-adamantyl)pyridine and 2-(2-adamantyl)pyridine are also observed. Oxidation of 2-adamantanol mediated by **1** affords only 6.9% of 2-adamantanone under identical conditions. Oxidation of adamantane by **1**/Zn/O$_2$ in CH$_3$CN/AcOH (10:1) yields low conversions of 1-adamantanol (2.8%), 2-adamantanol (1.2%), and 2-adamantanone (0.8%). Acceptable mass balances are larger than 95% in all cases.

These values are comparable to those previously reported[36a] for **1** and are further indicative of the equivalence of species **1**−**4** in catalytic solutions; this fact was anticipated due to the observed pyridine-dependent interconversions. The normalized 3°/2° preference on a per-hydrogen basis gives an average value of 2.65 for Gif-type oxidations. The selectivity for the tertiary position (3°/2° = 4.2) increases for oxidations in CH$_3$CN/AcOH, at the expense of lower yields achieved. These values can be compared with values of 11−48 for oxidation of adamantane by P-450 mimics (depending on porphyrin substitution) coupled to PhIO,[69] 20 for generic radical reactions of adamantane,[70] 10 for radical reactions (t-BuO$^\bullet$) of adamantane in pyridine[29] (albeit 2.7 for chlorination with t-BuOCl),[31b] 10 for oxidation of adamantane by Fe$_2$O(2,2′-bipy)$_4$(H$_2$O)$_2$(ClO$_4$)$_4$/t-BuOOH in CH$_3$CN,[15b] 9.5 for oxidation of adamantane by [FeCl$_2$(TPA)](ClO$_4$)/t-BuOOH (or CumOOH) in CH$_3$CN/C$_6$H$_6$ (1:1),[13c] 3−10 for oxidation of adamantane by Mn-porphyrin/KHSO$_5$

(65) (a) Mashuta, M. S.; Webb, R. J.; McCusker, J. K.; Schmitt, E. A.; Oberhausen, K. J.; Richardson, J. F.; Buchanan, R. M.; Hendrickson, D. N. *J. Am. Chem. Soc.* **1992**, *114*, 3815−3827. (b) Nie, H.; Aubin, S. M. J.; Mashuta, M. S.; Wu, C.-C.; Richardson, J. F.; Hendrickson, D. N.; Buchanan, R. M. *Inorg. Chem.* **1995**, *34*, 2382−2388.

(66) Reem, R. C.; Solomon, E. I. *J. Am. Chem. Soc.* **1987**, *109*, 1216−1226.

(67) (a) Miller, J. S., Ed. In *Extended Linear Chain Compounds*; Plenum: New York, 1983; Vol. 3. (b) Kahn, O. *Molecular Magnetism*; VCH: New York, 1993; pp 251−286. (c) Bonner, J. C. In *Magneto-Structural Correlations in Exchange Coupled Systems*; Willett, R. D., Gatteschi, D., Kahn, O., Eds.; D. Reidel: Dordrecht, The Netherlands, 1985; pp 157−205.

(68) (a) Bórras-Almenar, J. J. Doctoral Dissertation, University of Valencia, 1992. (b) The numerical parameters used in the analytical expression ($A = 1.35365$, $B = -0.317459$, $C = 4.20982$, $D = 24.7699$, $E = -4.96588$) were computed by the group in Florence: Gatteschi, D. Unpublished results.

(69) Groves, J. T.; Nemo, T. E. *J. Am. Chem. Soc.* **1983**, *105*, 6243−6248.

(70) (a) Murahashi, S.-I.; Oda, Y.; Naota, T. *J. Am. Chem. Soc.* **1992**, *114*, 7913−7914. (b) Fukunishi, K.; Tabushi, I. *Synthesis* **1988**, 826−827. (c) Fossey, J.; Lefort, D.; Massoudi, M.; Nedelec, J.-Y.; Sorba, J. *Can. J. Chem.* **1985**, *63*, 678−680.

(or magnesium monoperphthalate) catalytic systems,[71] 4.0 for oxidation of adamantane by $Fe(PA)_2/H_2O_2$ (1:16) in py/AcOH (2:1),[36c] 3.5 for oxidation of adamantane by $Fe_2O(OAc)_2Cl_2$-$(2,2'$-bipy$)_2$ (or $Fe_2O(OAc)(tmima)_2(ClO_4)_3/H_2O_2$ in CH_3CN,[16] 3 for oxidation of adamantane (1-ol, 50%; 2-ol, 50%) by sMMO,[37b] 2.2 for oxidation of adamantane by Fe_2O-$(HB(pz)_3)_2(OAc)_2/Zn/O_2$ in $CH_2Cl_2/AcOH$ (400/1),[18] and ~2 for generic oxidation of alkanes by $HO^•$.[72]

The intermolecular deuterium KIE values (k_H/k_D) obtained by oxidation of a mixture of adamantane/adamantane-d_{16} (1:1) under Gif conditions at 298 K are as follows for each product: 2.01(12) (2-adamantanone), 0.92(4) (2-adamantanol), 1.18(3) (1-adamantanol), 1.18(6) (4-(1-adamantyl)pyridine), and 1.25-(2) (2-(1-adamantyl)pyridine). These values are comparable to those reported[73] for the oxidation of cyclohexane to cyclohexanone (KIE = 2.3) by Gif^{IV}-type systems, but substantially lower than intramolecular KIE values obtained from P-450-[5a,41] or sMMO-catalyzed oxidations,[27a,42] although similar to intermolecular KIE values (≤ 2) associated with P-450 oxidations.[5a] Typically, the KIE value for oxidations by $HO^•$ is 1.[72] However, values close to unity, as some of those obtained in the present competitive intermolecular experiments are, may be the outcome of a rate-determining step not related to the C−H(D) bond-cleavage process. This can be true, for instance, for 2-adamantanol assuming that it is produced by rate-determining reduction of a common M−OOC(H)R₂ precursor via O−O cleavage. Importantly, the KIE value for cyclohexanol has been shown[73] to substantially increase in the presence of PPh_3 in the catalytic mixture. Hydrogen abstraction to yield the ketone is expected to be facile, hence KIE values for the ketone is largely influenced by the initial C−H cleavage.

Oxidation of adamantane by $1/H_2O_2$ (20 equiv) in py/AcOH (10:1) under N_2 affords only traces of 2-(1-adamantyl)pyridine (<0.2%). At 150 equiv of H_2O_2, minor amounts of products are observed: 0.4% (2-adamantanone), 0.3% (2-adamantanol), 0.4% (1-adamantanol), and 0.2% (2-(1-adamantyl)pyridine) ($3°/2° = 2.6$). The reactions are accompanied by evolution of O_2 (monitored by virtue of an oxygen-sensitive Clark electrode), apparently generated by catalase-type decomposition of H_2O_2. Similar catalytic oxidations with H_2O_2 under O_2 afford minor amounts of oxo products: 2-adamantanone (0.5%) and 1-adamantanol (0.6%) ($3°/2° = 3.6$). Identical results were obtained by employing the $3/H_2O_2$ combination. The analogous oxidation with $1/t$-BuOOH (dry, 20 equiv) affords low yields of 4-(1-adamantyl)pyridine (4.0%) and 2-(1-adamantyl)pyridine (4.7%) anaerobically and minor amounts of oxo products under O_2: 2-adamantanone (0.2%), 2-adamantanol (0.15%), and 1-adamantanol (0.5%) ($3°/2° = 4.6$). Catalytic oxidation with peracetic acid affords only traces of products. Apparently, none of these oxo donors provide viable alternatives to the Zn/O_2 system. The catalase-type reaction has been noted by the Barton group in conjunction with catalytic reactions mediated by the $FeCl_3/H_2O_2$ system in the absence of PAH in neat pyridine[29,74] and by the present $1/H_2O_2$ combination in py/AcOH (10:1) in oxidations of cyclohexane.[75]

Oxidation of isopentane (17.19 mmol) by the $1/Zn/O_2$ combination yields the following oxo products: 2-methyl-2-butanol (0.05 mmol), 3-methyl-2-butanol (0.01 mmol), 3-methyl-2-butanone (0.17 mmol), 3-methyl-1-butanol (0.001 mmol), isovaleraldehyde (0.04 mmol), 2-methyl-1-butanol (0.003 mmol), and 2-methylbutyraldehyde (0.08 mmol). The normalized 3°/2°/1° preference of 3.6/6.5/1.0 indicates a net preponderance for the oxygenation of the secondary position and a small, but not negligible, activation of the primary C−H bonds. Oxidation of 2-methyl-1-butanol and 3-methyl-1-butanol under similar conditions affords only traces of the corresponding aldehydes. The oxidation of isopentane by sMMO from *M. trichosporium* OB3b has been carefully studied[37a] to reveal exclusive formation of isopentanols. The product distribution indicates that there is a net preference for the production of tertiary alcohol in the absence of regulatory component B, but that primary alcohols are strongly favored in oxidations with the fully reconstituted enzyme.

Oxidation of benzene by the $1/Zn/O_2$ system in py/AcOH (10:1) affords very low yields of phenol (0.3%) and no biphenyl (major product[72] of oxidation by genuine $HO^•$ along with phenol). Oxidation of toluene by the same system provides very low conversions to the following products: benzaldehyde (0.7%), benzyl alcohol (0.6%), benzoic acid (0.4%), *o*-cresol (0.2%), *m*-cresol (0.1%), *p*-cresol (0.1%), bibenzyl (trace). Noteworthy is the fact that genuine hydroxyl radicals add to the phenyl ring almost exclusively (97%; $k = 3.0 \times 10^9 M^{-1} s^{-1}$).[72] Oxidation of *cis*-stilbene provides mostly benzaldehyde (29.6%) and small amounts of *trans*-stilbene oxide (2.4%) and deoxybenzoin (0.2%). This finding may argue against the presence of high-valent iron−oxo species similar in function to those postulated in biological oxygenases. However, metal−oxo entities more akin to $[MnO_4]^{-}$ [76] and RuO_4[77] in terms of reactivity can potentially cleave C=C bonds oxidatively.

Oxidation of pyridine (33.4 mmol) in the absence of other substrates by the system $1/Zn/O_2$ in py/AcOH (10:1) yields 2-HOpy (0.11 mmol), 3-HOpy (0.07 mmol) and 4-HOpy (0.01 mmol), as quantified by ^{1}H NMR. In addition, 2,2′-bipy (0.01 mmol) and 2,4′-bipy (0.05 mmol) have been detected and evaluated by GC. Reportedly,[29] pyridine (33 mL) is oxidized by $FeCl_3$ (1 mmol)/PAH (4 mmol)/H_2O_2 (4 mmol) to afford 2-HOpy (1.04 mmol) and 3-HOpy (0.30 mmol) but only traces of 4-HOpy. The system $Fe(PA)_2$(10 mM)/H_2O_2(10 mM) in py/AcOH (2:1) yields 3-HOpy as the primary product.[20b] In contrast, we note that $HO^•$ addition to pyridine in pulse radiolysis experiments affords 2-HOpy$^•$ and 4-HOpy$^•$ (2:1).[72,78] In addition to the corresponding hydroxypyridines, these initial radicals can yield bipyridines via a dimerization/dehydration process.[72] Finally, hydroxyl radicals, generated by photolysis of *N*-hydroxy-2-thiopyridinone in py/AcOH, have been reported to yield hydroxylation products 2-HOpy/3-HOpy/4-HOpy in a ratio of 13.0/1.0/5.9.[79]

The Nature of Active Oxidant(s) in Gif-Type Chemistry. The most unresolved issue in conjunction with Gif-type oxidations concerns the active oxidant involved. In principle, for O_2- or H_2O_2-based oxidations, this could be a high-valent iron−oxo unit and/or hydroxyl radicals. Structural evidence presented in this investigation reinforces the argument that there exist

(71) Hoffmann, P.; Robert, A.; Meunier, B. *Bull. Soc. Chim. Fr.* **1992**, *129*, 85−97.

(72) (a) Buxton, G. V.; Greenstock, C. L.; Helman, W. P.; Ross, A. B. *J. Phys. Chem. Ref. Data* **1988**, *17*, 513−886. (b) Baker, R. R.; Baldwin, R. R.; Walker, R. W. *Trans. Faraday Soc.* **1970**, *66*, 2812−2826. (c) Russell, G. A. In *The chemistry of alkanes and cycloalkanes*; Patai, S., Rappoport, Z., Eds.; Wiley: New York, 1992; pp 966−983. (d) Kochi, J. K. In *Free Radicals*; Kochi, J. K., Ed.; Wiley: New York, 1973; Vol. II, pp 689−690.

(73) Barton, D. H. R.; Doller, D.; Geletii, Y. V. *Tetrahedron Lett.* **1991**, *32*, 3811−3814.

(74) Barton, D. H. R.; Hu, B.; Taylor, D. K.; Rojas Wahl, R. U. *Tetrahedron Lett.* **1996**, *37*, 1133−1136.

(75) Barton, D. H. R. Personal communication.

(76) (a) Fatiadi, A. J. *Synthesis* **1987**, 85−127. (b) Gardner, K. A.; Mayer, J. M. *Science* **1995**, *269*, 1849−1851.

(77) (a) Lee, D. G.; van den Engh, M. In *Oxidation in Organic Chemistry, Vol. 5*; Trahanovsky, W. S., Ed.; Academic Press: New York, 1973; Part B, Chapter IV, pp 177−227. (b) Torii, S.; Inokuchi, T.; Kondo, K. *J. Org. Chem.* **1985**, *50*, 4980−4982. (c) Carlsen, P. H. J.; Katsuki, T.; Martin, V. S.; Sharpless, K. B. *J. Org. Chem.* **1981**, *46*, 3936−3938.

(78) Cercek, B.; Ebert, M. *Trans. Faraday Soc.* **1967**, *63*, 1687−1698.

(79) Barton, D. H. R.; Bévière, S. D.; Chavasiri, W.; Doller, D.; Liu, W.-G.; Reibenspies, J. H. *New J. Chem.* **1992**, *16*, 1019−1029.

ferrous sites in Gif-type solutions which bear intriguing similarities to the diiron site in H_{red} of sMMO. As demonstrated in the structural features of **4**, the documented lability of pyridine favors oxygen-rich ligation by acetato moieties which, in turn, may better precondition the diferrous site for dioxygen activation. Indeed, on a qualitative basis compound **4** reacts with dioxygen much more readily than species **3**. The relative importance of oxygen- versus nitrogen-rich ligation has been noted in conjunction with structural and functional features of the diiron center in hemerythrin[80] (oxygen carrier in a nitrogen-rich environment) and sMMO[6a,b] (oxygen activator in an oxygen-rich environment). Interestingly, products of autoxidation include "as isolated" diferric species such as $[Fe_2ZnO-(O_2CCH_3)_6(py)_3] \cdot py$ (**1″**) which exhibit more than one analogies with the corresponding diiron sites in H_{ox} of sMMO. Of greater significance, however, would be to characterize the precursor intermediates generated by the interaction of the ferrous sites with dioxygen as suggested by preliminary UV−vis spectra.

The importance of structural parameters to guide further analysis of metal-centered events notwithstanding, functional characteristics are more relevant to the mode of action of the active oxidant involved and potentially revealing with respect to its nature. The product profiles and intermolecular KIE values obtained from Gif-type oxidations in the present study share aspects of, but are not completely consistent with, oxidations performed by genuine hydroxyl radicals (generated by pulse radiolysis)[72] or high-valent iron−oxo species, as the latter have been known from studies involving P-450 isozymes/mimics or sMMO. It is worth noting, however, that only in the case of sMMO has a reasonably well-characterized Fe^{IV}_2-$(\mu$-O$)_2$ unit been detected,[4b,c] while the elusive Fe^{IV}=O/residue$^{+\bullet}$ moiety of P-450 is believed to have a long-lived analogue in the form of the isolable peroxidase compound I.[81]

It can be argued that the enhanced preference for the activation of the secondary positions of adamantane by comparison to typical radical reactions is nevertheless compatible with the action of the most indiscriminate radicals, including HO$^\bullet$ (3°/2° ≈ 2−2.5).[72] On the other hand, isopentane and other substrates (methylcyclohexane,[47] methylcyclopentane,[47] *trans*-decalin,[47] 3-ethylpentane,[82] 1,4-*trans*-dimethylcyclohexane[83]) show a net preference for the oxygenation of the secondary position, a result that needs to be confirmed with a wider selection of substrates. However, the following observations make the presence of free hydroxyl radicals *as the sole active oxidant* improbable: (i) alcohols (2-adamantanol, isopentanols) are oxidized to the corresponding aldehydes and ketones only to a limited extent; indeed, alcohols are inferior substrates by comparison to the parent alkanes; (ii) toluene is mostly oxidized at the alkyl substituent rather than via addition to the aromatic ring, albeit at low conversions; (iii) products of pyridine oxidation by the present system are not consistent with those obtained from hydroxyl radical oxidations; and (iv) reportedly,[22] primary positions remain largely unaffected under Gif-type conditions, although the present results with isopentane call for a wider evaluation of the oxygenation at primary sites. The low conversions of benzene to phenol cannot be fully assessed, but do not exclude the presence of low fluxes of hydroxyl radicals, unless the active oxidant is capable of activating the aromatic ring. The fact that hydrogen peroxide, a reagent that may have a higher propensity to generate hydroxyl radicals,

does not initiate a viable shunt pathway may also speak against a dominant role for HO$^\bullet$ in the present system. The same result can also be interpreted as indicating absence of ferric peroxo units, generated by the interaction of ferrous sites with dioxygen. However, hydrogen peroxide and dioxygen are most likely acting at substantially different iron centers. Indeed, the μ-oxo compound **1** may be better predisposed to mediate catalase-type activity, as judged by structural similarities with the metal site of manganese-containing catalases[84] and iron-based catalase mimics.[85] Interestingly, the all-ferric $[Fe_3O(O_2CCH_3)_6(H_2O)_3]^+$ has been recently shown[86] to generate the trisperoxo compound $[Fe_6(O)_2(O_2)_3(O_2CCH_3)_9]^-$ upon interaction with H_2O_2.

Similarly, the potent oxidant in Gif solutions does not display typical characteristics of high-valent iron−oxo species, as those are commonly invoked in explaining the activity of P-450 and sMMO. However, the absence of model systems bearing genuine (per)ferryl units and the only recently emerging[4] physicochemical characterization of the iron−oxo moiety in the biological oxygenases poses limitations to the generality of the comparative assessment. Nevertheless, the present system neither mediates epoxidation of olefinic substrates nor does it exhibit analogous chemo- and regioselectivity toward aliphatic hydrocarbons by comparison to the biological oxygenases. Admittedly, the influence of the protein environment in modulating chemo/regioselection may superimpose on the intrinsic ability of the putative iron−oxo moiety to bring about a given transformation. The small 3°/2° and KIE values calculated in the present study cannot be easily reconciled with an iron−oxo unit abstracting a hydrogen atom from a C−H bond via a more or less linear transition state, unless its potency is such that resembles the indiscriminate activity of hydroxyl radicals. A side-on C−H approach to a putative Fe=O moiety would be more consistent with the observed values, but the paucity of primary carbons remains problematic in both cases.

Of great interest in this context will be the exploration of the conditions that influence the formation and govern the lifetime of substrate radicals, potentially generated in oxidations mediated by the **1**/Zn/O_2 system.[87] With the exception of a limited number of substrates (adamantane being one of them), Barton has concluded[29] (on the basis of extensive radical-scavenging studies applied to the FeCl$_3$/PAH/H_2O_2 oxidizing system) that Gif-type oxidations do not involve alkyl radicals (concerted C−H activation), unless a circumstantial Fenton-type Fe^{II}/H_2O_2 system preponderates. In a study comparing the same Gif system (as well as the one employing *t*-BuOOH) with P-450 and sMMO, Newcomb has suggested[38] that Gif-type oxidation of diagnostic radical-clock substrates indicates the presence of diffusively free alkyl radicals, as opposed to short-lived (<100 fs) substrate radicals generated by the action of the biological oxygenases. Although these studies do not directly reveal the nature of the active oxidant responsible for hydrogen abstraction, they are nonetheless suggestive of a fundamental difference in the mode of C−H activation by Gif-type systems and their biological counterparts. It remains to be seen whether this difference is solely due to the intrinsic characteristics of the

(80) (a) Stenkamp, R. E. *Chem. Rev.* **1994**, *94*, 715−726. (b) Wilkins, P. C.; Wilkins, R. G. *Coord. Chem. Rev.* **1987**, *79*, 195−214.

(81) (a) Sundaramoorthy, M.; Terner, J.; Poulos, T. L. *Structure (London)* **1995**, *3*, 1367−1377. (b) Ortiz de Montellano, P. R. *Annu. Rev. Pharmacol. Toxicol.* **1992**, *32*, 89−107.

(82) Barton, D. H. R.; Doller, D.; Ozbalik, N.; Balavoine, G.; Gref, A. *Tetrahedron Lett.* **1990**, *31*, 353−356.

(83) Barton, D. H. R.; Chavasiri, W. *Tetrahedron* **1997**, *53*, 2997−3004.

(84) (a) Varynin, V. V.; Vagin, A. A.; Melik-Adamyan, V. R.; Grebenko, A. I.; Khangulov, S. V.; Popov, A. N.; Andrianova, M. E.; Vainshtein, B. K. *Dokl. Akad. Nauk. SSSR* **1986**, *288*, 877−880. (b) Pecoraro, V. L.; Gelasco, A.; Baldwin, M. J. In *Mechanistic Bioinorganic Chemistry*; Thorp, H. H., Pecoraro, V. L., Eds.; American Chemical Society: Washington, DC, 1995; pp 265−301. (c) Penner-Hahn, J. E. In *Manganese Redox Enzymes*; Pecoraro, V. L., Ed.; VCH Publishers: New York, 1992; pp 29−45. (d) Wieghardt, K. *Angew. Chem., Int. Ed. Engl.* **1989**, *28*, 1153−1172.

(85) Maurer, B.; Crane, J.; Schuler, J.; Wieghardt, K.; Nuber, B. *Angew. Chem., Int. Ed. Engl.* **1993**, *32*, 289−291.

(86) Shweky, I.; Pence, L. E.; Papaefthymiou, G. C.; Sessoli, R.; Yun, J. W.; Bino, A.; Lippard, S. J. *J. Am. Chem. Soc.* **1997**, *119*, 1037−1042.

(87) Work in progress in collaboration with M. Newcomb.

respective oxo donor/C−H acceptor couples or whether the protein envelope has some major role to play in the latter cases.

Alternative active oxidants that need to be further considered are disguised forms of the two extreme candidates. These may include metal- or residue-bound hydroxyl radicals, as for instance in $Fe^{II/III}$−O···OH[30] or HO•pyN/pyN•OH[88] and their dioxygen adducts thereof, as well as metal−(per)oxo units bearing configurations more suitable for ketonization processes (for instance, *cis*-FeO$_2$ moieties).[89]

A dominant Fe^{II}/O_2^- interaction—as opposed to an Fe^{II}/H_2O_2 alternative—has been suggested to be operational in Gif^{IV} systems on the basis of control experiments[29,36a] and electrochemical studies.[90] Although the intermediacy of superoxo moieties is indisputable in dioxygen activation, their generation is more likely to occur in the facile reduction of O_2 at Fe(II) sites rather than as part of the sluggish reaction of dioxygen with Zn. In contrast, Zn can easily reduce Fe(III) centers to their Fe(II) counterparts. That the Fe^{II}/O_2 interaction in the present system is important for catalytic turnovers has also been suggested both by the observed suppression of all product yields on increasing dioxygen pressure (most likely due to overstabilization of the ferric components) and by the complete cessation of catalytic activity with the trifluoroacetate analogue system $[Fe_3O(O_2CCF_3)_6(H_2O)_3]/Zn/O_2$ in py/CF$_3$COOH (10:1), owing to the stability of $Fe^{II}(O_2CCF_3)_2(py)_4$ with respect to dioxygen.[91] Interestingly, the latter system becomes productive with excess H_2O_2 replacing the Zn/O$_2$ combination. These observations indicate that the iron environment influences the outcome of catalysis and may play a prominent role, rather than merely acting as a decomposition center of organoperoxides.

Conclusions

The following are the principal findings of this study:

(1) Reduction of basic iron or iron/zinc acetates under Gif-type conditions generates a host of mononuclear, oligonuclear, and polymeric chain ferrous and zinc species which are implicated in pyridine-dependent equilibria; the $[Fe^{II}(O_2CCH_3)_2(py)_4]$ (**3**)/$[Fe^{II}_2(O_2CCH_3)_4(py)_3]_n$ (**4**) interconversion dominates in py/AcOH solutions, although the exact nature of **4** in solution is not presently known.

(2) Upon exposure to dioxygen or air, the Fe(II)/Zn(II) sites eventually regenerate the basic acetate structure $[Fe_2M^{II}O$-$(OAc)_6(py)_3]$·py, the divalent site M(II) being occupied by a statistical mixture of Fe and Zn. Depending on the initial concentration of the ferrous component, intermediates are observed that need to be further characterized. Otherwise, these consistent chemical redox cycles (mediated by a variety of reducing agents and dioxygen) may be responsible for sustaining the catalytic conversions of Gif chemistry.

(3) Analogies with structural elements of the diiron site in H$_{red}$ or H$_{ox}$ of sMMO are apparent in $[Fe^{II}_2(O_2CCH_3)_4(py)_3]_n$ (**4**) and $[Fe_2Zn^{II}O(OAc)_6(py)_3]$·py (**1″**), respectively. However, the nuclearity of the present system upon chemical redox cycles is not conserved.

(4) Product profiles and KIE values obtained from catalytic oxidation of a number of substrates reveal features that are not fully consistent with corresponding characteristics assigned to HO•-based oxidations or to sMMO/P-450 oxygenase activity due to high-valent iron−oxo moieties. Shunt pathways involving H$_2O_2$ lead to oxygen evolution rather than substrate oxygenation.

Future studies directed toward exploring the nature and kinetics of intermediates generated in both metal- and substrate-centered events will address specifically whether a novel oxidant is involved or hydroxyl radicals and/or (per)ferryl units are present in disguise.

Supporting Information Available: Mössbauer spectrum (4.2 K) of a polycrystalline sample of **1′** with theoretical fit, plot of molar susceptibility (χ_M) per ferrous ion and effective magnetic moment (μ_{eff}, with best fit) as a function of temperature for compound **11**, tables containing numerical values of measured and calculated molar susceptibility and effective magnetic moment versus temperature for **4** and **11**, and tables containing listings of crystal and data collection parameters, atomic coordinates and isotropic thermal parameters, interatomic distances, bond angles, and anisotropic displacement parameters for **1′**, **1″**, and **2**−**11** (95 pages). See any current masthead page for ordering and Internet access instructions.

JA970562R

(88) An early proposal by Shilov favored generation of electrophilic pyNO$^+$: Geletii, Y. V.; Lavrushko, V. V.; Shilov, A. E. *Dokl. Akad. Nauk. SSSR* **1986**, *288*, 139−143.

(89) Ferrate(V,VI)-like species cannot be excluded, especially for oxidations with H$_2O_2$, although oxidation of primary and secondary alcohols is expected to occur readily. See: (a) Rush, J. D.; Bielski, B. H. J. *Inorg. Chem.* **1989**, *28*, 3947−3951. (b) Sharma, V. K.; Bielski, B. H. J. *Inorg. Chem.* **1991**, *30*, 4306−4310.

(90) (a) Barton, D. H. R.; Sobkowiak, A. *New J. Chem.* **1996**, *20*, 929−932. (b) Balavoine, G.; Barton, D. H. R.; Boivin, J.; Gref, A.; Le Coupanec, P.; Ozbalik, N.; Pestana, J. A. X.; Rivière, H. *Tetrahedron* **1988**, *44*, 1091−1106. (c) Balavoine, G.; Barton, D. H. R.; Boivin, J.; Gref, A.; Hallery, I.; Ozbalik, N.; Pestana, J. A.; Rivière, H. *New J. Chem.* **1990**, *14*, 175−183.

(91) Tapper, A.; Long, J. R.; Stavropoulos, P. Manuscript in preparation.